



Review

# A review of hot deformation behavior and constitutive models to predict flow stress of high-entropy alloys



Zeinab Savaedi<sup>1</sup>, Reza Motallebi<sup>1</sup>, Hamed Mirzadeh \*

School of Metallurgy and Materials Engineering, College of Engineering, University of Tehran, P.O. Box 11155-4563, Tehran, Iran

## ARTICLE INFO

### Article history:

Received 8 December 2021

Received in revised form 19 January 2022

Accepted 23 January 2022

Available online 26 January 2022

### Keywords:

Multi-principal element alloys

Hot deformation

Mechanical properties

Constitutive analysis

Flow stress

## ABSTRACT

This review article summarizes the hot deformation behavior of high entropy alloys (HEAs) and the corresponding constitutive description of flow stress. The potential of hot working for grain refinement via dynamic recrystallization (DRX), reduction of casting defects, and enhancement of mechanical properties of HEAs is explained. The necklace formation, work hardening analysis for identification of the occurrence and initiation of DRX, and the effects of processing parameters on dynamically recrystallized grain size are discussed. The effects of deformation conditions (represented by the Zener-Hollomon parameter), alloying elements, dynamic precipitation, and the presence of phases on the hot deformation behavior and restoration processes of DRX and dynamic recovery (DRV) are overviewed. The application of processing maps for the characterization of the onset of flow instability, cracking, flow softening, and DRX during hot forming of HEAs is presented. Regarding the constitutive modeling of flow stress for characterization of material flow (at different deformation temperatures, strain rates, and strain), the utilization of the threshold stress (due to the presence of phases or their precipitation during high-temperature deformation), and temperature-dependent Young's modulus, as well as correlating the obtained values of deformation activation energy and stress exponent with the expected ones from the creep theories are taken into account. Afterward, the available methods and equations for modeling and prediction of flow curves during thermomechanical processing are assessed, where the strain-compensated Arrhenius model, artificial neural network (ANN) model, Zerilli-Armstrong model, Johnson-Cook model, Hensel-Spittel model, and dislocation density-based multiscale constitutive model are presented. Finally, some suggestions for future research works are proposed.

© 2022 Elsevier B.V. All rights reserved.

## Contents

1. Introduction .....	2
2. Enhancement of mechanical properties by hot working .....	3
3. Hot deformation behavior .....	4
3.1. Effect of deformation temperature .....	4
3.2. Dynamic recrystallization .....	5
3.3. Processing maps .....	8
3.4. Phase transformations during hot deformation .....	8
4. Constitutive description of material flow .....	9
4.1. Typical constitutive analysis .....	9
4.2. Physically-based constitutive analysis .....	11

\* Corresponding author.

E-mail address: [hmirzadeh@ut.ac.ir](mailto:hmirzadeh@ut.ac.ir) (H. Mirzadeh).

5.	Modeling and prediction of flow stress . . . . .	12
5.1.	Arrhenius model . . . . .	12
5.2.	ANN model . . . . .	12
5.3.	Zerilli-Armstrong model . . . . .	13
5.4.	Johnson-Cook model . . . . .	13
5.5.	Hensel-Spittel model . . . . .	14
5.6.	Dislocation density-based model . . . . .	15
6.	Discussion and future directions . . . . .	15
7.	Summary . . . . .	17
	Funding body . . . . .	18
	Data Availability . . . . .	18
	Declaration of Competing Interest . . . . .	18
	References . . . . .	18

## 1. Introduction

High-entropy alloys (HEAs) containing at least five principal elements in an equal or near-equal atomic percentage with no apparent difference between the solute and solvent have been introduced in 2004 by Yeh et al. [1] and Cantor et al. [2], which exhibit high mixing entropy that promotes the formation of random solid-solution phases instead of intermetallic compounds. Despite their room-temperature state regarding the formation of single phase or multiple phases, HEAs can be defined as alloys with a configurational entropy in a random state equal or larger than  $1.5R$ , where  $R$  is the gas constant. Alternatively, HEAs may be defined as alloys with at least five principal elements, each with an atomic percentage between 5 and 35 [3]. Accordingly, satisfying one of these criteria is considered to be enough for an alloy to be regarded as a HEA [4].

For  $n$  constituting elements and atomic fraction of  $c_i$  for each element, the configurational entropy of mixing per mole ( $\Delta S_{\text{conf}}$ ) can be expressed as follows [4,5]:

$$\Delta S_{\text{conf}} = -R \sum_{i=1}^n c_i \ln c_i \quad (1)$$

Despite HEAs with  $\Delta S_{\text{conf}} \geq 1.5R$ , alloys having  $1.0R < \Delta S_{\text{conf}} < 1.5R$  can be considered as medium-entropy alloys (MEAs). However, the consideration of quaternary equimolar alloys as HEAs (with 4 constituting elements and  $\Delta S_{\text{conf}} = 1.386R$ ) has loosened the restrictions of both definitions. On the other hand, due to the increased chance of phase formation between binary elements, a true solid solution might not be determined simply by increasing  $n$ , and hence  $\Delta S_{\text{conf}}$ . In fact, many HEAs contain different phases such as Laves phases or numerous topologically close-packed (TCP) phases, designated as the  $\mu$ ,  $\chi$ , and  $\sigma$  [6]. Accordingly, a more general term such as multi-principal element alloys

(MPEAs), complex concentrated alloys (CCAs), and multi-component alloys (MCAs) might also be used for referring to these alloys [4].

For designing the chemical composition of HEAs, some other considerations should be taken into account. The thermodynamic parameter ( $\Omega$ ) can be defined as the ratio of product of the mixing entropy ( $\Delta S_{\text{mix}}$ ) and the melting temperature ( $T_m$ ) to the absolute value of the mixing enthalpy ( $\Delta H_{\text{mix}}$ ) [7]:

$$\begin{aligned} \Omega &= T_m \Delta S_{\text{mix}} / |\Delta H_{\text{mix}}| \\ \Delta H_{\text{mix}} &= \sum_{i=1, i \neq j}^n 4 \Delta H_{\text{mix}}^{ij} c_i c_j \\ T_m &= \sum_{i=1}^n c_i (T_m)_i \end{aligned} \quad (2)$$

where  $\Delta H_{\text{mix}}^{ij}$  is the mixing enthalpy for the binary equiatomic element<sub>i</sub>element<sub>j</sub> alloy. A large value of  $\Omega$  favors the formation of a single-phase random solid solution according to the thermodynamics principles. The Hume-Rothery rules have been considered by introducing specific composition-weighted terms for differences in atom radii ( $\delta$ ) and electronegativity, and for an average valence electron concentration (VEC) [4]:

$$\delta = \left\{ \sum_{i=1}^n c_i (1 - r_i / \sum_{i=1}^n c_i r_i)^2 \right\}^{0.5} \quad (3)$$

where  $r_i$  are the atomic radius for each element. As can be deduced from Fig. 1, the conditions of  $-15 < \Delta H_{\text{mix}} < 5 \text{ kJ/mol}$ ,  $1.1 \leq \Omega$ , and  $\delta \leq 6.6$  favor the formation of the solid-solution phase [7].

The HEAs show a unique combination of properties, such as high strength (even at elevated temperatures) and strength-to-weight ratio [8], good fracture resistance (even at cryogenic temperatures) [9], excellent thermal stability [10], good superplasticity [11], high wear resistance [12] and corrosion resistance [13], and desirable magnetic properties [14]. However, due to the inherent compositional complexity and the huge difference in the melting points

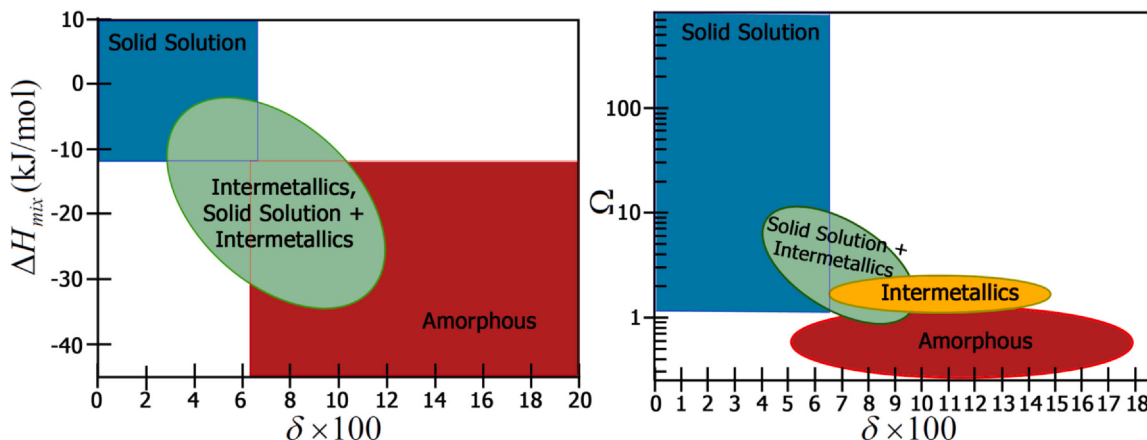


**Fig. 1.** Empirical correlations to separate phase regions (Redrawn based on [3,7]).

between the constituent elements in HEAs, significant elemental segregation and phase formation might occur during solidification and cooling [15], which necessitates high cooling rates and subsequent hot working in the solid state (extrusion, rolling, and forging) [16]. In this respect, the presence of coarse columnar grain and casting defects are a major problem, which can be relieved by hot working.

Moreover, a vast majority of HEAs are designed for elevated temperature applications [8]. Furthermore, similar to other metallic materials, hot deformation is one of the main processing routes to obtain required shapes and for microstructural refinement by dynamic recrystallization (DRX) [17]. Accordingly, investigation of the hot deformation behavior of HEAs is one of the hot topics of this research field. The characterization of hot flow behavior is important for designing the metalforming processes, where proper constitutive relationships are often used to describe the flow behavior in computer codes to model the hot deformation response of the parts under the prevailing loading conditions [18]. Therefore, the present review summarizes the hot deformation behavior of HEAs and the corresponding methods for constitutive modeling of flow stress.

Accordingly, in the following sections, firstly, the importance of hot working for enhancing the mechanical properties of HEAs is summarized. Afterward, the hot deformation behavior of HEAs is critically discussed with emphasis on the restoration processes at elevated temperature, microstructural evolutions, constitutive analysis, and prediction of hot flow curves. Finally, the future prospects in this research field are proposed.

## 2. Enhancement of mechanical properties by hot working

Casting defects and the presence of coarse columnar structures in the as-cast HEAs are responsible for poor ductility/strength combination. Grain refinement is a viable approach to overcome this limitation [19]. For grain refinement of HEAs, a combination of cold/warm working and heat treatment for static recrystallization (SRX) is typically used. For this technique, the grain size is generally on the order of several micrometers, and hence, the severe plastic deformation (SPD) techniques are used to achieve very fine grain sizes. However, a small volume of material can be processed [20], and most SPD-processed HEAs exhibit low ductility levels because of the significant reduction in work hardening and the saturation of defect

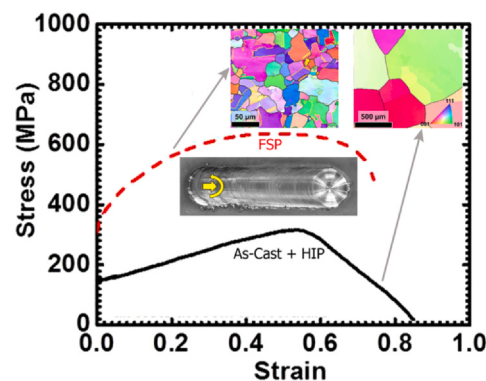


**Fig. 3.** Tensile properties and microstructures of  $\text{Al}_{0.1}\text{CoCrFeNi}$  HEA in the as-cast+HIP (hot isostatic pressing) and FSP-processed conditions [27].

densities after processing [21]. An effective and industrially applicable method for refining the grains of HEAs is hot deformation by utilization of DRX [20]. An example is shown in Fig. 2 [21,22], where it can be seen that the hot extrusion process is an effective way for grain refinement and enhancement of the strength and ductility of CoCrFeMnNi HEA compared to the as-cast counterpart. It can be seen that the processing of the extruded alloy by ECAP led to submicron grain size and further increase in the strength level.

Sluggish diffusion at the hot deformation temperature might lead to significant grain refinement [23]. Similar to the effect of hot extrusion, the enhancement of mechanical properties has been reported for hot rolled C-doped CoCrFeMnNi HEA [24] and C-doped FeNiMnAlCr HEA [25], and for hot forging [26].

Friction stir processing (FSP) applies severe plastic deformation at elevated temperatures, which can refine the grain size by DRX. This technique has also been applied to HEAs for the enhancement of mechanical properties. For instance, Kumar et al. [27] studied the effect of FSP on the as-cast  $\text{Al}_{0.1}\text{CoCrFeNi}$  HEA. The coarse initial grain size (on the order of millimeters) was refined to  $\sim 14\ \mu\text{m}$  with an enhancement of mechanical properties, as shown in Fig. 3 [27].

The effect of hot deformation on the powder metallurgy parts made of HEAs is also significant. For instance, for the  $\text{TiNbTaZrAl}$  HEAs, Fig. 4 [28] reveals that the amount of porosity decreases by increasing the compressive deformation at  $800\ ^\circ\text{C}$  and  $0.001\ \text{s}^{-1}$ ; and hence, the relative density increases. This is one of the well-known effects of hot working, which might be important for the actual application of the parts.

Thermomechanical processing and severe plastic deformation of HEAs can be used for grain refinement and achieving a microstructure that exhibits superplastic behavior at the hot working temperatures ( $T > 0.5T_m$ ) [29], and the topic has been comprehensively reviewed recently [11]. Superplasticity is the ability of a polycrystalline material to exhibit, in a generally isotropic manner, very high elongations prior to failure (at least 400%) [30]. Grain boundary sliding (GBS) is the primary deformation mechanism, for which a strain rate sensitivity index ( $m$ ) of  $\sim 0.5$  has been reported. For instance, Shaysultanov et al. [31] studied the superplasticity of  $\text{AlCrCuNiFeCo}$  HEA after multiaxial forging (MAF) at  $950\ ^\circ\text{C}$ . The effect of MAF on grain refinement is shown in Fig. 5. While at  $800\ ^\circ\text{C}$ , the total elongation is below 400%, superplastic ductilities have been achieved at  $900\ ^\circ\text{C}$  and  $1000\ ^\circ\text{C}$ , as shown in Fig. 5. The retention of the fine-grained microstructure at elevated temperature is an important issue, where the complexity of the microstructure is favorable to inhibit grain growth at a high temperature of  $1000\ ^\circ\text{C}$ . Moreover, by increasing the deformation temperature, the peak elongation has been achieved at higher optimum strain rates, which is vital for superplastic forming from the industrial standpoint [32].

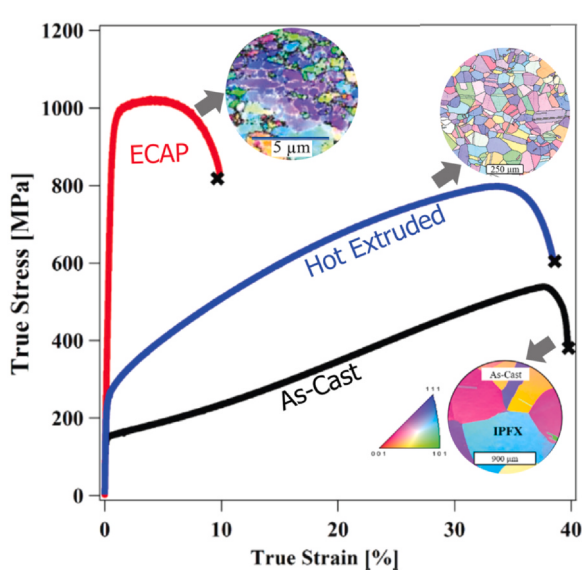


**Fig. 2.** Tensile properties and microstructures of  $\text{CoCrFeMnNi}$  HEA in the as-cast, as-extruded, and ECAP-processed conditions [21,22].

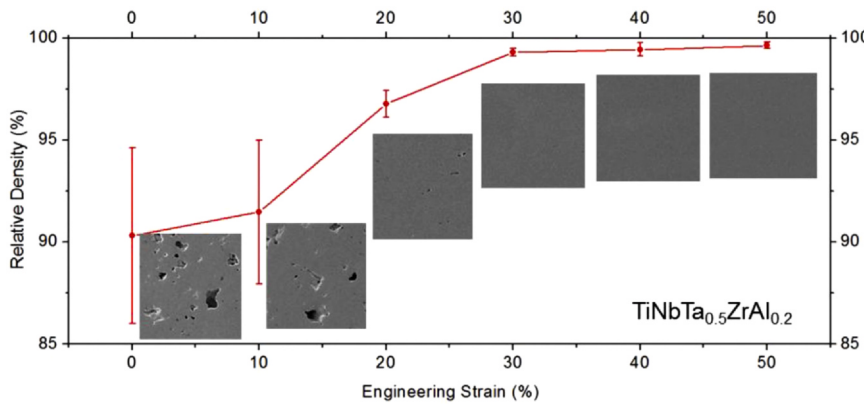


**Fig. 4.** Relative density of  $\text{TiNbTa}_{0.5}\text{ZrAl}_{0.2}$  HEAs after compressive deformation at  $800\text{ }^\circ\text{C}$  and  $0.001\text{ s}^{-1}$  [28].

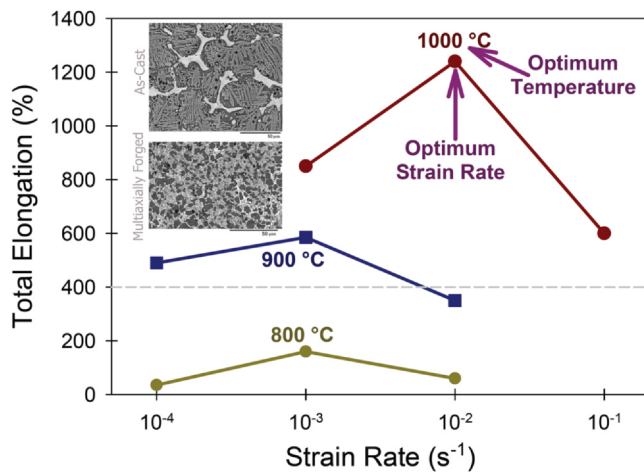


**Fig. 5.** Elongation diagrams of  $\text{AlCrCuNiFeCo}$  HEA [31].

It is quite important to understand the hot deformation behavior and microstructural evolutions during high-temperature thermo-mechanical processing of HEAs, which is treated in the next Section.

### 3. Hot deformation behavior

#### 3.1. Effect of deformation temperature

The deformation temperature greatly affects the mechanical properties of HEAs. For instance, Lin et al. [33] studied the effect of deformation temperature on the yield stress of  $\text{CrMnFeCoNiAl}_{0.75}$  HEA. The addition of Al into the single-phase  $\text{CrMnFeCoNi}$  Cantor alloy promotes the formation of face-centered cubic (FCC) + body-centered cubic (BCC, Cr-Fe-rich phase) + B2 (Ni-Al-rich phase) multi-phase structure as shown in Fig. 6. It can be seen that the Al addition has led to the remarkable enhancement of yield stress compared to the  $\text{CrMnFeCoNi}$  Cantor alloy, which can also be compared to the well-known superalloys, as shown in Fig. 6. Based on the figure, the yield stress drops suddenly at temperatures higher than  $\sim 0.4T_m$  ( $540\text{ }^\circ\text{C}$ ). This is in accordance with the expectations for hot working, where the thermally activated dislocation motion and the decreased strength of B2 and BCC phases are responsible for this behavior [33].

The elevated-temperature tensile behavior of hot-rolled  $\text{CrMnFeCoNi}$  HEA has been reported by Jang et al. [34]. The FCC structure was retained in the hot deformed state. A notable temperature sensitivity of the yield stress was recorded, as shown in Fig. 7. Due to the low stacking fault energy (SFE) of  $\sim 20\text{--}25\text{ mJ/m}^2$ , DRX was the predominant restoration mechanism, as shown in the

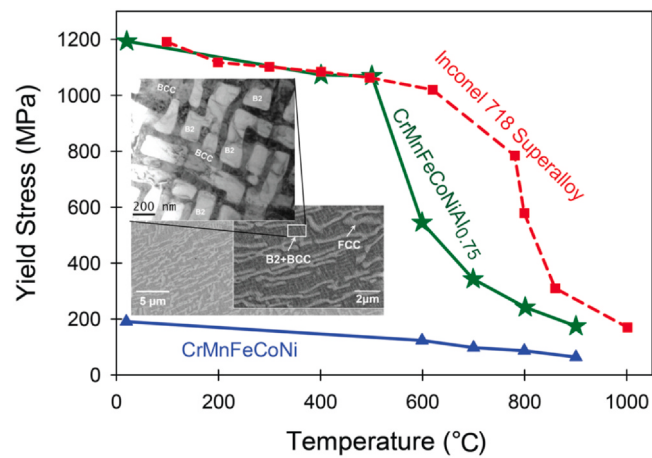


**Fig. 6.** Yield stress of  $\text{CrMnFeCoNiAl}_{0.75}$ ,  $\text{CrMnFeCoNi}$ , and Inconel 718 superalloy versus deformation temperature, as well as the microstructures of the  $\text{CrMnFeCoNiAl}_{0.75}$  HEA [33].

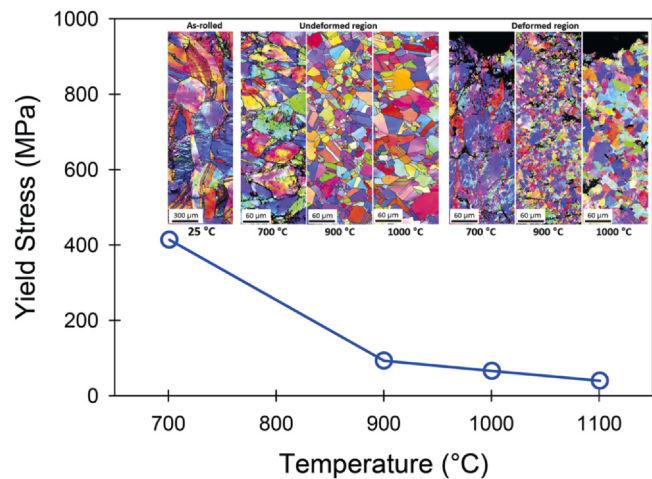


**Fig. 7.** Yield stress of hot rolled  $\text{CrMnFeCoNi}$  HEA versus deformation temperature, as well as some representative microstructures [34].

microstructures of the deformed region in Fig. 7. The complete DRX has been achieved at  $900$  and  $1000\text{ }^\circ\text{C}$ . The microstructures of the undeformed regions are also shown in Fig. 7, which reveals that the static recrystallization also led to the refinement of grains. However,

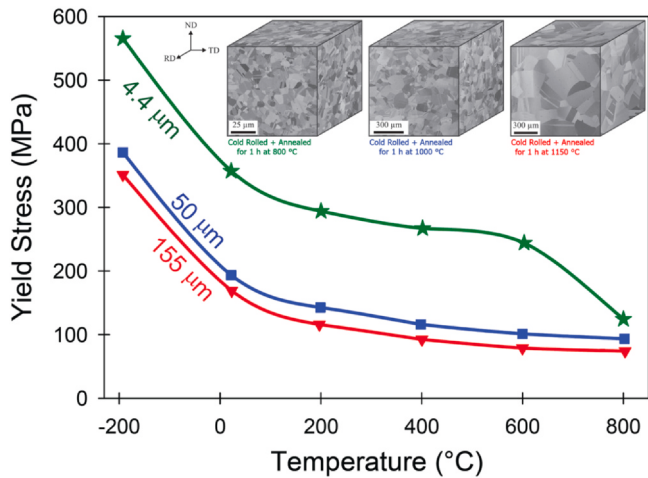


**Fig. 8.** Yield stress of CoCrFeMnNi HEA versus deformation temperature, as well as some representative 3D microstructures [35].

it can be seen that the potential of DRX for grain refinement is superior to that of SRX [34].

Otto et al. [35] processed the CoCrFeMnNi alloy by cold rolling and annealing at different temperatures for 1 h to obtain various grain sizes and subsequently studied the dependence of the yield stress on the deformation temperature. The results are shown in Fig. 8, where it can be seen that the yield stress shows a strong dependency on the temperature. Moreover, the grain size dependency of the yield stress is also significant, which is related to the well-known dependency of the strength on the grain size as represented by the Hall-Petch relationship. However, at temperatures higher than  $0.5T_m$  (such as 800 °C), the grain size dependency of the yield stress becomes negligible, which can be verified by the sudden drop of flow stress from 600° to 800°C. It is in accordance with the well-known fact stating that at hot working regime with the usual mechanism of glide and climb of dislocations (dislocation creep), the dependency of flow stress on grain size is low [36].

### 3.2. Dynamic recrystallization

Hot deformation and DRX behavior of CoCrFeNiMn HEA have been studied by Stepanov et al. [37]. The necklace DRX mechanism was found to be responsible for the evolution of microstructure during DRX, as it is evidenced by electron backscatter diffraction (EBSD) maps shown in Fig. 9a. The obtained fraction recrystallized and DRX grain size ( $d_{DRX}$ ) are also shown in Fig. 9a. It can be seen that by increasing the deformation temperature at a constant strain rate of 0.001 s<sup>-1</sup> and strain of 1.4, the recrystallized fraction increases, and the size of DRX grains increases. The latter effect can be better presented via consideration of the dependency of the steady state flow stress ( $\sigma_S$ ) and grain size in Fig. 9b, where a straight line can be fitted to this double logarithmic plot [37]. Accordingly, the following well-known relationship of can be used to model the data ( $A$  and  $q$  are constants) [38]:

$$\sigma_S = Ad_{DRX}^{-q} \quad (4)$$

The increase in the recrystallization fraction and DRX grain size by increasing the deformation temperature and decreasing strain rate has also been reported by Eleti et al. [23], Jeong et al. [39], and Patnamsetty et al. [40] for CoCrFeNiMn HEA, Jeong et al. [41] for Al<sub>0.7</sub>CoCrFeMnNi, and Wang et al. [42] for Al<sub>0.7</sub>NiCoFeCr. It is noteworthy that the eutectic HEAs such as Al<sub>0.7</sub>CoCrFeMnNi show the most effective grain refinement during hot deformation, which could be attributed to the small initial grain size, particle stimulated

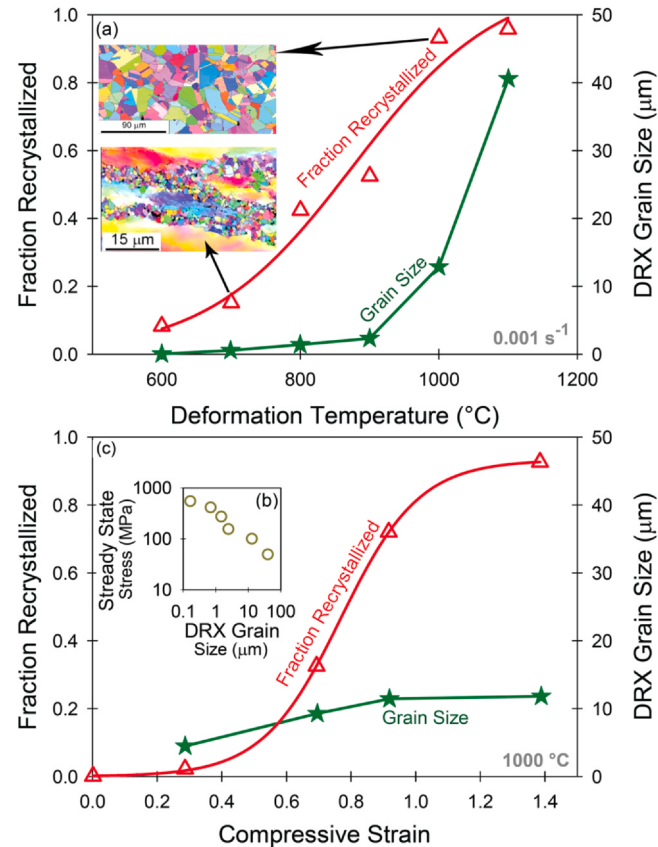


**Fig. 9.** DRX kinetics and grain size for hot deformed CoCrFeNiMn HEA [37].

nucleation (PSN) effect of the fragmented BCC particles, and high localized deformation at the interfaces of BCC/FCC in the eutectic microstructure [41].

Based on Stepanov et al. [37], the kinetics of DRX at 1000 °C is shown in Fig. 9c, representing the classical S-curve [37]. The change in the DRX grain size with strain seems to be insignificant, which is a characteristic feature of the necklace DRX mechanism (the growth of each grain stops by the concurrent deformation) [43]. For HfNbTa-TiZr refractory HEA, Eleti et al. [44] clearly showed this effect, as depicted in Fig. 10 by EBSD maps and the corresponding plots.

According to Fig. 10, grain boundary bulging is responsible for the formation of fine grains in the necklace mechanism. It should be noted that subgrain structures composed of low-angle grain boundaries were observed in the regions adjacent to the necklace DRX grains, as indicated by black arrows. The formation of equiaxed DRX grains resulting from grain boundary bulging is one of the typical processes for the formation of necklace structures, as also shown by transmission electron microscopy (TEM) images of Fig. 11 for MoNbTaTiV HEA [45]. The formation of necklace structure has also been shown for refractory Ti<sub>2</sub>ZrMo<sub>0.5</sub>Nb<sub>0.5</sub> HEA [46].

For alloys with low SFE, the rate of dynamic recovery (DRV) is low and cannot counteract the work hardening rate. Therefore, the increased dislocation density might lead to the initiation of DRX at a critical strain ( $\epsilon_C$ ) corresponding to a critical stress ( $\sigma_C$ ) [43,47,48]. The inflection points in the plots of the work hardening rate ( $\theta = d\sigma/d\epsilon$ ) versus  $\sigma$  can be used to obtain  $\sigma_C$ . These inflection points are equivalent to a minimum on the plot of  $-d\theta/d\sigma$  versus  $\sigma$  [43,48,49]. The application of this technique for HEAs has been verified by Annasamy et al. [19] for Al<sub>x</sub>CoCrFeNi HEAs, Wang et al. [42] for NiCoFeCrAl<sub>0.7</sub>, Kahnooji et al. [50] for Fe<sub>53</sub>Mn<sub>27</sub>C<sub>10</sub>Cr<sub>10</sub> HEA, Alijani et al. [51] for FECoNiMnV HEA, and Sajadi et al. [52] for

<sup>1</sup> Zeinab Savaedi and Reza Motallebi have equally contributed to this work

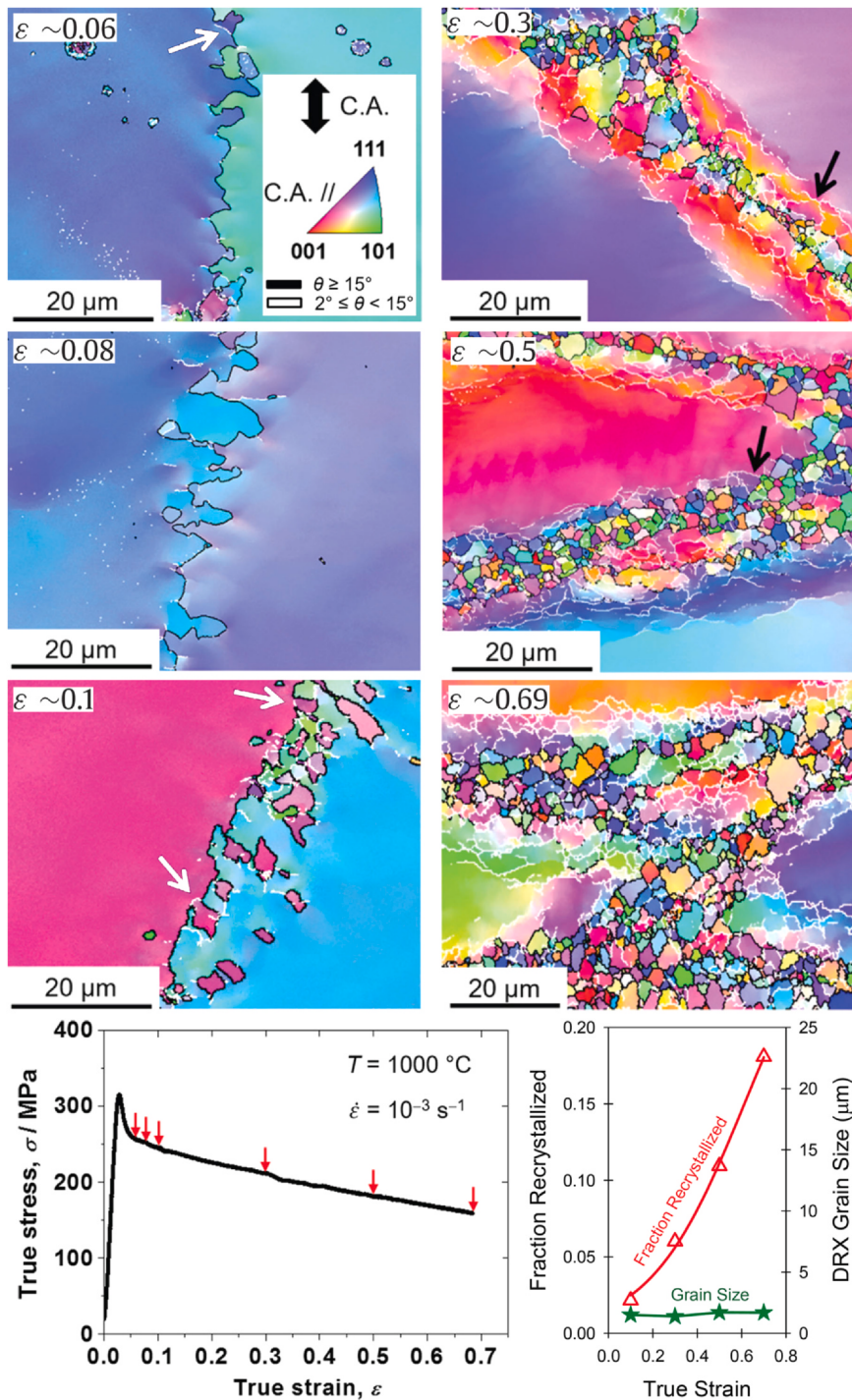


**Fig. 10.** EBSD maps, DRX kinetics, and grain size for HfNbTaTiZr HEA [44]. White arrows are low-angle grain boundaries bridging bulged initial grain boundaries, while black arrows correspond to subgrains.

FeCrCuNi<sub>2</sub>Mn<sub>2</sub> HEA. For Al<sub>0.3</sub>CoCrFeNi HEA, the flow curves and representative plots of  $-d\theta/d\sigma$  versus  $\sigma$  are shown in Fig. 12 [19].

Flow curves at 980 and 1030 °C under low strain rates showed a typical DRX behavior, characterized by flow softening after the peak point. A broadened peak was observed with no steady-state region (Fig. 12a). The flow stress at 980 and 1030 °C under a strain rate of 0.01 s<sup>-1</sup> increased progressively without showing a peak flow stress (Fig. 12a) [19]. However, work hardening rate analysis in Fig. 12b reveals that the 1030 °C-0.01 s<sup>-1</sup> sample shows a clear minimum in

the plots of  $-d\theta/d\sigma$  versus  $\sigma$ , which reveals the occurrence of DRX. The obtained DRX fractions are summarized in Fig. 12b, where low fractions of DRX have been recorded for this sample, and hence, a much higher strain is required to achieve a large DRX fraction.

Sometimes, a small amount of a particular alloying element is added to HEAs to alter their properties. These additions might also significantly affect the hot deformation behavior. For instance, Yi et al. [53] investigated the effect of doping by carbon (0.1 wt%) and nitrogen (0.05 wt%) on the hot compression behavior of

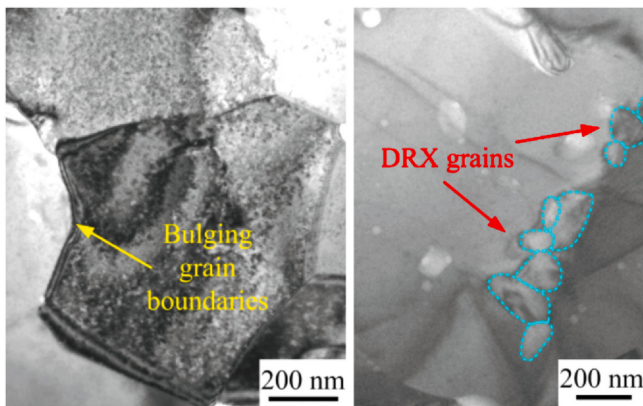


Fig. 11. TEM images of bulging and DRX grain formation in MoNbTaTiV HEA [45].

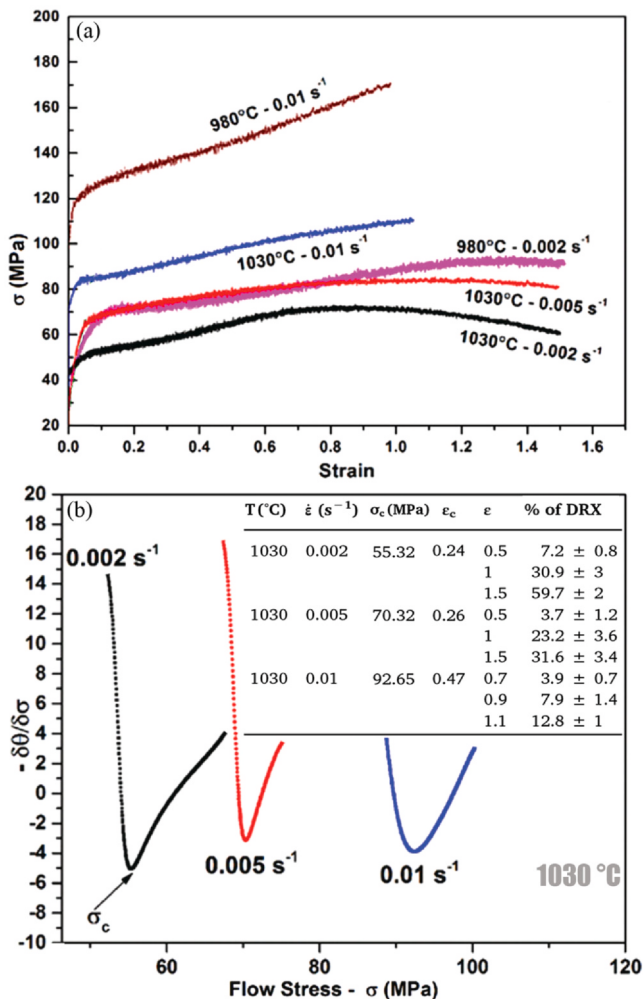


Fig. 12. Flow curves and the plots of  $-\frac{d\theta}{d\sigma}$  versus  $\sigma$  for  $\text{Al}_{0.3}\text{CoCrFeNi}$  HEA [19].

$\text{Co}_{45}\text{Cr}_{25}\text{Fe}_{15}\text{Ni}_{15}$  HEA. The results are summarized in Fig. 13, where it can be seen that both DRX fraction and grain size strongly depend on the doped element.

Doping with N led to the lower DRX fractions at low temperatures, while its retardation effect decreased by increasing the deformation temperature. However, at high temperatures, where the DRX fraction is high for the N-doped alloy, a much finer DRX grain size is achieved compared to the C-doped alloy [53]. Therefore,

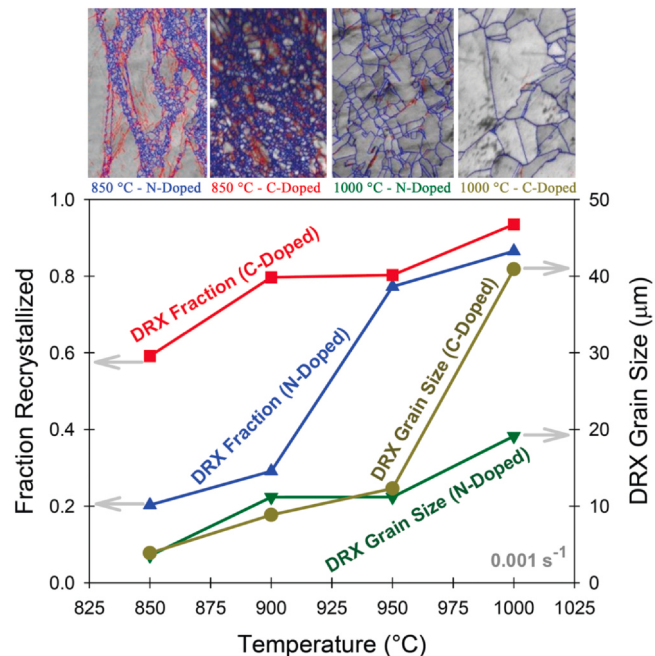


Fig. 13. DRX fraction and grain size of C- and N-doped  $\text{Co}_{45}\text{Cr}_{25}\text{Fe}_{15}\text{Ni}_{15}$  HEA [53].

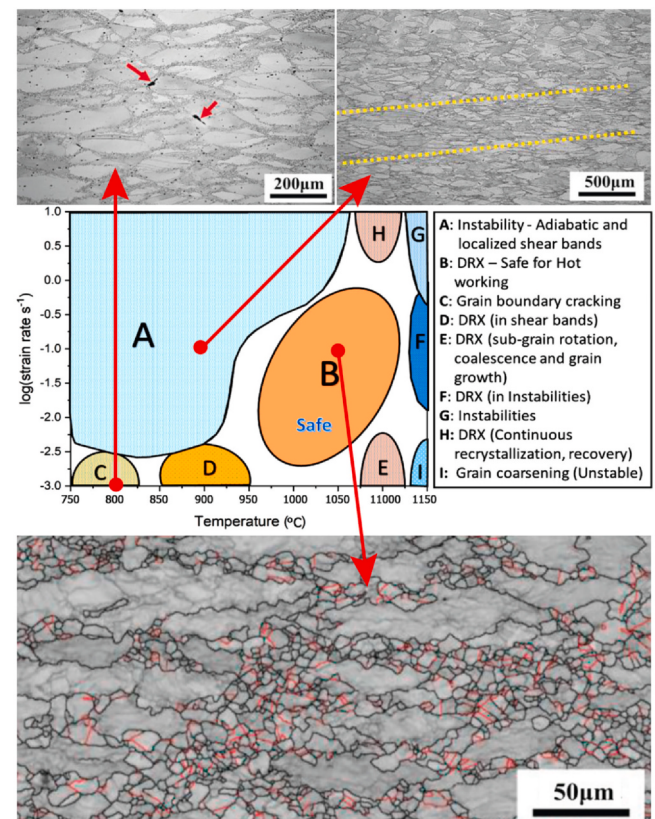
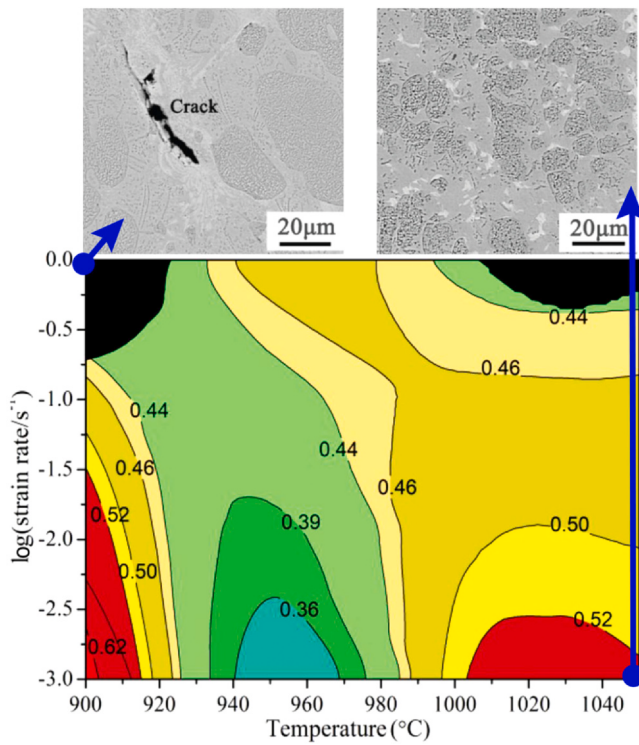


Fig. 14. Processing map of  $\text{CoCrFeMnNi}$  HEA at true strain of 0.6 [56].

N-doping has led to a finer grain size in this alloy. Similar DRX grain size refining effect has been reported by Wang et al. [54] for CrFe-CoNi alloy via Mo addition, which is related to the pinning action of Mo-rich  $\sigma$  phase particles. In another study, the effect of C-doping on



**Fig. 15.** Processing map of AlCrCuFeNi HEA at true strain of 0.6 [57].

the hot deformation behavior of Fe<sub>40</sub>Mn<sub>40</sub>Co<sub>10</sub>Cr<sub>10</sub> HEA has also been investigated by Tang et al. [55], where the effect of M<sub>23</sub>C<sub>6</sub> type carbide has been noted.

### 3.3. Processing maps

Hot working behavior and processing map of CoCrFeMnNi HEA has been investigated by Patnamsetty et al. [56]. The developed processing map is shown in Fig. 14, delineating various deterministic domains, including those of cracking processes and unstable flow, thus enabling the identification of a safe processing window for the hot working of the alloy. For instance, the microstructure of region A reveals the presence of shear bands and flow instability. In contrast, safe region B reveals the occurrence of DRX. As another example, region C is characterized by grain boundary cracking, as shown in Fig. 14. It was also argued that flow softening behavior might occur due to the onset of flow instability and cracking, and hence, it might not be appropriate to investigate the hot working behavior only based on the shape of the flow curves [56].

As another example, the processing maps for the equiatomic AlCrCuFeNi HEA have been developed by Wang et al. [57], where an example is shown in Fig. 15. It can be seen that in the instability regime (black regions), hot working has led to obvious cracking. However, in the region with a high power dissipation efficiency (red region), a uniform distribution of phases can be seen, where high power dissipation efficiency regions are safe ones for hot working [57]. For CoCrCu<sub>1.2</sub>FeNi HEA, Jiang et al. [58] proposed processing maps for hot working and argued that the asynchronous DRX of the two phases makes the boundary of FCC<sub>1</sub> and FCC<sub>2</sub> easier to crack, leading to the formation of hot working defects [58]. For AlCrCuNi-FeCo HEA, the regions of flow instability associated with adiabatic shear banding and cracking have also been characterized by Prasad et al. [59] for CoCuFeMnNi.

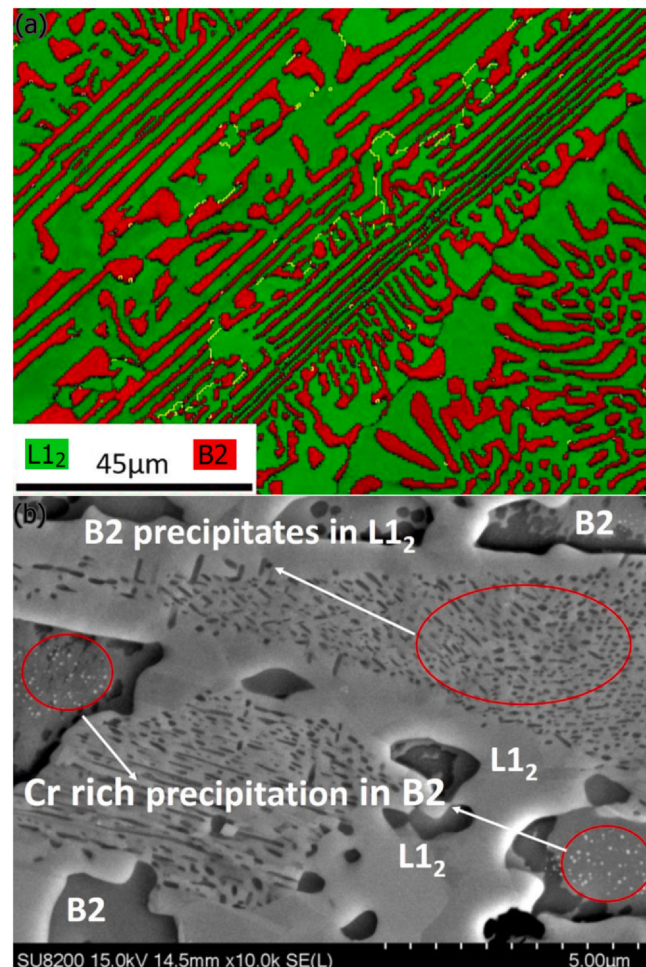


**Fig. 16.** Microstructure of AlCoCrFeNi<sub>2.1</sub> eutectic HEA: (a) as-cast alloy and (b) after hot compression at 800 °C-0.0001 s<sup>-1</sup> [60].

### 3.4. Phase transformations during hot deformation

Hot deformation of an AlCoCrFeNi<sub>2.1</sub> eutectic HEA (with the microstructure shown in Fig. 16a) has been studied by Zaid Ahmed et al. [60]. DRX was the main mechanism for controlling the microstructural evolutions at higher temperatures. However, the dominant restoration mechanism at lower temperatures was identified as DRV, for which dynamic precipitation played a critical role in the inhibition of DRX. In this case, as shown in Fig. 16b, precipitates in the L1<sub>2</sub> phase are rich in Ni and Al, whereas precipitates in the B2 phase are rich in Cr [60]. The suppression of DRX via precipitation has also been critically discussed by Zhang et al. [61].

Accordingly, precipitation in highly alloyed HEAs might be an important factor in determining the hot deformation behavior. In this respect, Tian et al. [62] attributed the flow softening to the dynamic precipitation and DRV in equiatomic AlCoCrFeNi HEA. As another example, the microstructural evolution in equiatomic AlCoCrFeNi HEA at 1100 °C has been compared for processes of annealing and hot compression by Lee et al. [63]. The results are shown schematically in Fig. 17. It can be seen that the high-temperature exposure leads to the formation of a soft FCC phase at the expense of the brittle disordered A2 BCC phase. However, the effect of hot compression is more significant, for which the homogeneous distribution of FCC phase and the significant grain

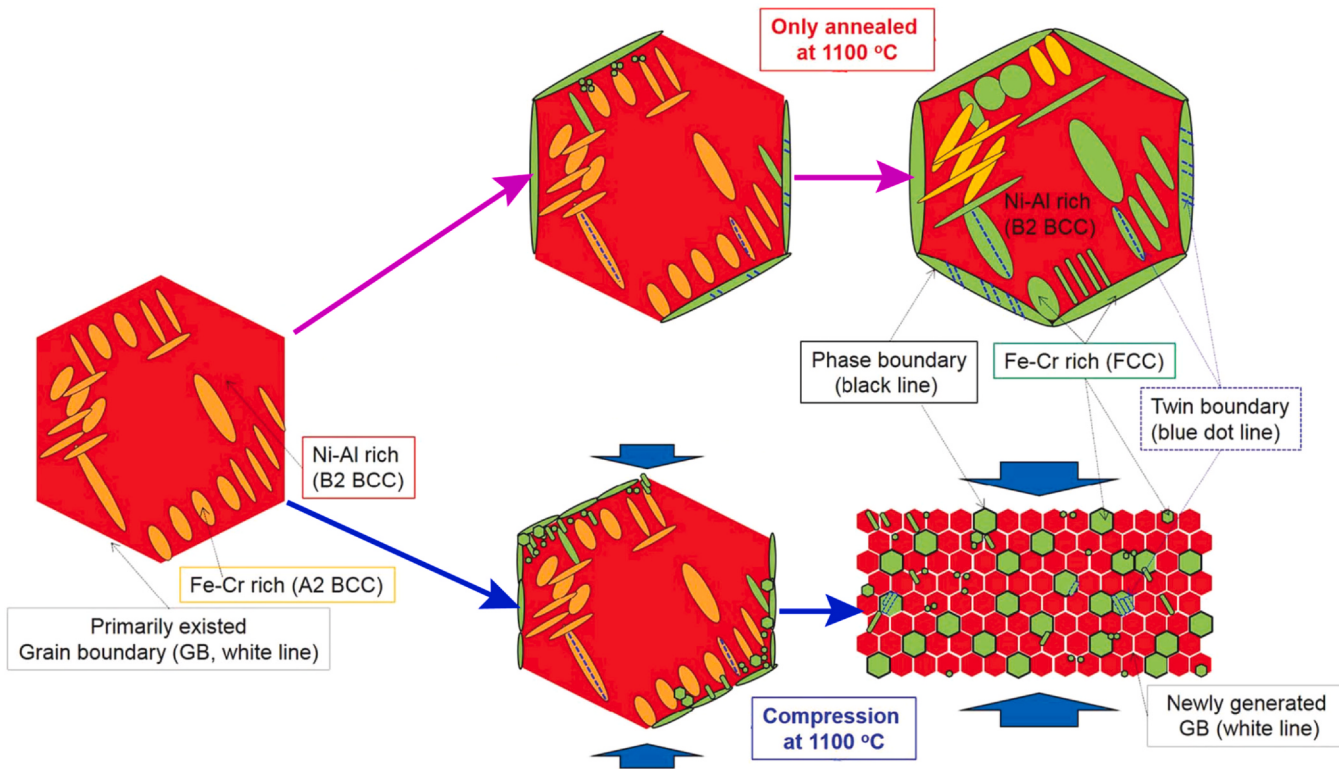


**Fig. 17.** Microstructural evolution in equiatomic AlCoCrFeNi HEA at 1100 °C for processes of annealing and hot compression [63].

refinement of B2 BCC matrix by DRX dominantly affect the softening and toughening of the material [63]. The DRX behavior of Al<sub>x</sub>CoCrFeNi duplex HEAs has also been studied in detail by Haghdadi et al. [64].

#### 4. Constitutive description of material flow

##### 4.1. Typical constitutive analysis

The Zener-Hollomon parameter ( $Z$ , as defined in Eq. 5) [65] can be related to the flow stress ( $\sigma$ ) in different ways, as summarized in Eq. (6) (power law), 7 (exponential law), and 8 (hyperbolic sine law) [66,67]:

$$Z = \dot{\varepsilon} \exp(Q/RT) \quad (5)$$

$$Z = A' \sigma^{n'} \quad (6)$$

$$Z = A'' \exp(\beta\sigma) \quad (7)$$

$$Z = A \{ \sinh(\alpha\sigma) \}^n \quad (8)$$

In these equations,  $A'$ ,  $A''$ ,  $A$ ,  $n'$ ,  $n$ ,  $\beta$ , and  $\alpha \approx \beta/n'$  are constants. Moreover,  $\dot{\varepsilon}$ ,  $T$ , and  $Q$  are the strain rate, temperature, and hot deformation activation energy, respectively. The stress multiplier  $\alpha$  is an adjustable constant that brings  $\alpha\sigma$  into the correct range, giving linear and parallel lines in  $\ln \dot{\varepsilon}$  versus  $\ln \{ \sinh(\alpha\sigma) \}$  plots [68,69]. While the power law is preferred for relatively low stresses and the exponential law is suitable for high stresses, the hyperbolic sine law can be used for a wide range of temperatures and strain rates.

By combining Eqs. (5 and 6), the equation of  $Z = \dot{\varepsilon} \exp(Q/RT) = A' \sigma^{n'}$  is obtained, which can be expressed as follows by taking the natural logarithm from both sides:

$$\ln \dot{\varepsilon} = \{ \ln A' - Q/RT \} + n' \ln \sigma \quad (9)$$

Accordingly, the slope of the plot of  $\ln \dot{\varepsilon}$  vs.  $\ln \sigma$  is equal to  $n'$ , where an example is shown in Fig. 18a for the hot compressed

CoCrFeMnNi HEA by Patnamsetty et al. [40]. Moreover, Eq. (9) can be rewritten as follows

$$\ln \sigma = \{ (1/n') (\ln \dot{\varepsilon} - \ln A) \} + (Q/n')(1/RT) \quad (10)$$

Accordingly, the slope of the plot of  $\ln \sigma$  vs.  $1/RT$  gives the value of  $Q/n'$ , and consequently  $Q$  [70,71]. The power law creep equation can be expressed as [72,73]:

$$\dot{\varepsilon} \propto \frac{GbD}{kT} \left( \frac{b}{d} \right)^p \left( \frac{\sigma}{G} \right)^{n'}; D \propto \exp(-Q/RT) \quad (11)$$

where  $G$  is the shear modulus,  $b$  is the magnitude of the Burgers vector,  $D$  is the diffusion coefficient,  $Q$  is the activation energy for the appropriate diffusion process, and  $\sigma$  is the stress. The usual deformation mechanism during hot deformation is dislocation creep (glide and climb of dislocations), for which the value of  $p$  is zero. Accordingly, the equation  $\dot{\varepsilon} \exp(Q/RT) = A' \sigma^{n'}$  becomes equivalent to Eq. (11), and there is a possibility for discussing the hot deformation mechanisms based on the values of  $Q$  and  $n'$ . For dislocation creep, two important mechanisms can be mentioned: (I) glide and climb of dislocations in the climb-controlled regime, where  $Q$  is the activation energy for the lattice diffusion ( $Q_l$ ), and  $n'$  is  $\sim 4.5$  or  $5$ ; (II) glide and climb of dislocations in the viscous glide regime, where  $Q$  is the activation energy for the interdiffusion of the solute (due to its preferential segregation around the moving dislocations), and  $n'$  is  $\sim 3$  [36,74].

By combining Eqs. (5 and 7), the equation  $Z = \dot{\varepsilon} \exp(Q/RT) = A'' \exp(\beta\sigma)$  is obtained, which can be expressed as follows by taking the natural logarithm from both sides:

$$\ln \dot{\varepsilon} = \{ \ln A'' - Q/RT \} + \beta\sigma \quad (12)$$

Accordingly, the slope of the plot of  $\ln \dot{\varepsilon}$  vs.  $\sigma$  is equal to  $\beta$ , where an example is shown in Fig. 18b. Accordingly, the value of  $\alpha \approx \beta/n'$  can be calculated.

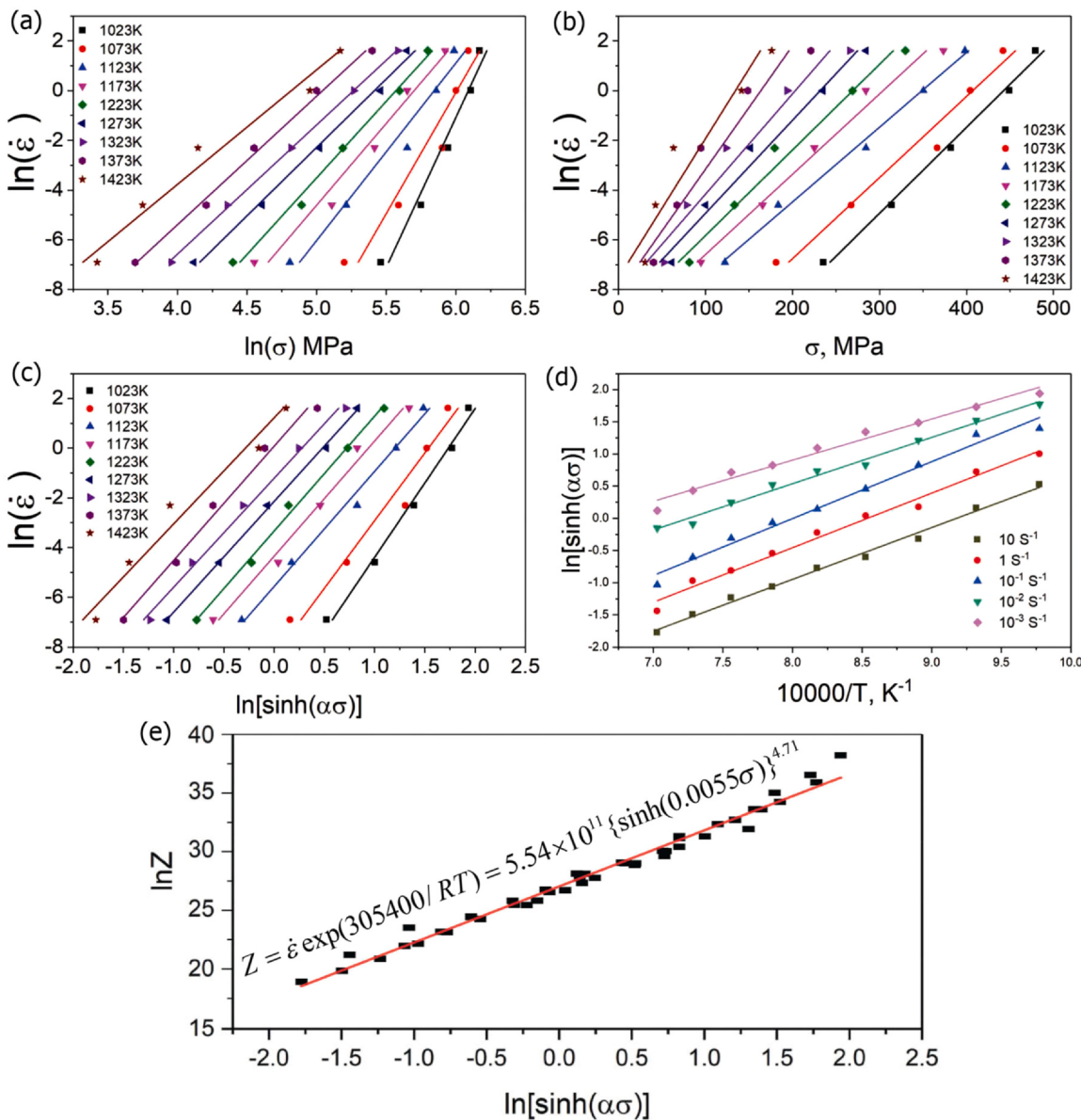


**Fig. 18.** Plots used for obtaining (a)  $n'$ , (b)  $\beta$ , (c)  $n$ , and (d)  $Q$ , as well as (e) the plot for constructing the final constitutive equation [40]. The data are related to the strain of 0.6.

Now, by combining Eqs. 5 and 8, the equation  $Z = \dot{\varepsilon} \exp(Q/RT) = A \{ \sinh(\alpha\sigma) \}^n$  is obtained, which can be expressed as follows by taking the natural logarithm from both sides:

$$\ln \dot{\varepsilon} = \{ \ln A - Q/RT \} + n \ln \{ \sinh(\alpha\sigma) \} \quad (13)$$

Accordingly, the slope of the plot of  $\ln \dot{\varepsilon}$  vs.  $\ln \{ \sinh(\alpha\sigma) \}$  is equal to  $n$ , where an example is shown in Fig. 18c. This equation can be rewritten as follows:

$$\ln \{ \sinh(\alpha\sigma) \} = \{ (1/n)(\ln \dot{\varepsilon} - \ln A) \} + (Q/Rn)(1/T) \quad (14)$$

Accordingly, the slope of the plot of  $\ln \{ \sinh(\alpha\sigma) \}$  vs.  $1/T$  gives the value of  $Q/Rn$ , where an example is shown in Fig. 18d. Based on equation  $Z = \dot{\varepsilon} \exp(Q/RT) = A \{ \sinh(\alpha\sigma) \}^n$ , the relation  $\ln Z = \ln A + n \ln \{ \sinh(\alpha\sigma) \}$  is determined. Based on all of the available data, the slope and intercept of the plot of  $\ln Z$  vs.  $\ln \{ \sinh(\alpha\sigma) \}$  can be used to obtain the final value on  $n$  and  $A$ , respectively. This can be used to construct the constitutive equation for describing the material, where an example is shown in Fig. 18e.

The reported parameters of the hyperbolic sine law for HEAs are summarized in Table 1. The regression analyses in different works are not similar, and hence, there is a wide range of values for parameters of the hyperbolic sine law in Table 1, which makes the comparison unreliable. However, in some cases, useful trends can be identified from the analysis of the data reported in Table 1. For instance, the average values of  $Q$  and  $n$  for the equiatomic CoCrFeMnNi alloy are  $(350+278.90+305.40)/3 = 311.76$  kJ/mol and  $(5.30+4.84+4.71)/3 = 4.95$ , respectively. The self-diffusion activation energies for Co, Cr, Fe, Ni, Mn are 288.5, 441.9, 284.12, 276.7, 288.4 kJ/mol, respectively [75,76]. Accordingly, the mean self-diffusion activation energy value is 315.92 kJ/mol, which is close to the experimental value of 311.76 kJ/mol. A related analysis has been performed by Jeong et al. [39], where the activation energy for the weighted diffusion coefficient calculated by weighting the contribution of each element in the CoCrFeMnNi HEA has been considered. It has been argued by Steurer [77] that the physical properties of HEAs are controlled to a large extent by the average of the properties of the

**Table 1**

Reported parameters of the hyperbolic sine law for HEAs.

Alloy (condition)	$\alpha$	$A$ ( $s^{-1}$ )	$n$	$Q$ (kJ/mol)	Reference
CoCrFeMnNi (Wrought)	0.0035	$2.36 \times 10^{15}$	5.30	350	[23]
	0.0068	$1.02 \times 10^{13}$	4.84	278.90	[78]
	0.0055	$5.54 \times 10^{11}$	4.71	305.40	[40]
CoCrFeMnNi <sub>0.007</sub> La <sub>0.0004</sub> (Wrought)	0.0068	$5.61 \times 10^{10}$	4.56	231.20	[78]
CoCrFeMnNi <sub>0.5</sub> (Homogenized)	0.0036	$5.83 \times 10^{14}$	8.07	362	[79]
Al <sub>0.4</sub> MnCrCoFeNi (Wrought)	0.0031	$1.38 \times 10^{19}$	6.86	522.02	[80]
CoCrFeNiTa (As-cast)	0.0043	$1.08 \times 10^{15}$	3.60	393.80	[81]
CoCrCu <sub>1.2</sub> FeNi (As-cast)	0.0059	$7.99 \times 10^{12}$	6.65	331.22	[58]
MoNbHfZrTi (As-cast)	0.0032	$6.6 \times 10^9$	2.88	326.11	[82]
Al <sub>0.5</sub> CoCrFeNi (As-cast)	0.0066	$1.8 \times 10^{10}$	7.19	293.83	[83]
Al <sub>0.5</sub> CoCrFeNi (Homogenized)	0.0066	$4.39 \times 10^{10}$	6.05	300.99	[83]
AlCoCrFeNi <sub>2.1</sub> (As-cast)	0.019	$7.2 \times 10^{11}$	2.5	336	[60]
AlCoCrFeNi (As-cast)	0.0057	$1.84 \times 10^{13}$	4.85	362	[62]
Al <sub>0.3</sub> CoCrFeNi (As-cast)	0.0037	$2.36 \times 10^{14}$	4.87	393.57	[84]
AlCrCuFeNi (As-cast)	0.0068	$7.12 \times 10^8$	3.66	199.13	[57]
CrFeCoNiMo <sub>0.2</sub> (Powder metallurgy)	0.0070	$1.77 \times 10^{17}$	3.73	463	[54]
C-doped CoCrFeNi (Homogenized)	0.0058	$1.97 \times 10^{20}$	5.72	526.07	[53]
N-doped CoCrFeNi (Homogenized)	0.0053	$1.42 \times 10^{12}$	4.69	334.68	[53]
CoCrFeNiZr <sub>0.1</sub> (As-cast)	0.0065	$4.8 \times 10^{12}$	3.40	329	[85]
FeCrCuNi <sub>2</sub> Mn <sub>2</sub> (As-cast)	0.0049	$3.96 \times 10^{30}$	12.22	708	[52]

constituting elements, which is consistent with the abovementioned analysis for the mean self-diffusion activation energy. Moreover, a similar approach has been used by Daryoush et al. [7], where the crystallization activation energy of mechanically alloyed AlFeCuZnTi high-entropy alloys during differential scanning calorimetry (DSC) thermal analysis (calculated based on the Kissinger equation) was correlated with the mean self-diffusion activation energy of the constituting elements. This kind of analysis regarding the deformation activation energy needs more attention to establish a basis for the future works.

It was shown above that the  $n$  value in this case is 4.95 on average, which is close to 5. Accordingly, based on both values of  $Q$  and  $n$ , the glide and climb of dislocations in the climb-controlled regime can be identified as the main deformation mechanism.

#### 4.2. Physically-based constitutive analysis

As discussed above, the usual hot deformation mechanism (glide and climb of dislocations in the climb-controlled regime) leads to  $n'$  of ~4.5 or 5, and  $Q = Q_1$  [72–74]. It has also been shown that the value of  $n$  in the hyperbolic sine equation can also be considered as 5. Moreover, these values, temperature-dependent Young's modulus ( $E$ ), and the diffusion coefficient ( $D$ ) can be incorporated into the hyperbolic sine law [86–88]:

$$\dot{\epsilon}/D_{(T)} = B [\sinh(\alpha'/\sigma/E_{(T)})]^5 \quad (15)$$

where the constants  $\alpha'$  and  $B$  are the modified stress multiplier and the hyperbolic sine constant, respectively. This equation might also be implemented by considering a variable  $n_E$  instead of 5. For instance, this equation has been applied for CoCrFeMnNi HEA by Jeong et al. [39], AlCoCrFeMnNi HEA by Jeong et al. [89], and Al<sub>0.5</sub>CoCrFeMnNi HEA by Kim et al. [90]. By consideration of deformation mechanisms, the activation energy for the plastic flow associated with the solute drag creep was estimated to be 251 kJ/mol for Al<sub>0.5</sub>CoCrFeMnNi HEA at low strain rates and high temperatures, which most likely represents the activation energy for the diffusivity of Al in the alloy. However, dislocation climb creep and power law breakdown (PLB) occurred at high strain rates and low temperatures, where the activation energy for plastic flow was 306.6 kJ/mol [90]. The transition of the solute drag creep to dislocation climb creep to PLB by increasing the flow stress has also been studied in detail by He et al. [76] for FeCoNiCrMn, and Jeong et al. [91,92] for Sn<sub>0.5</sub>CoCrFeMnNi and Al<sub>0.5</sub>CoCrFeMnNi.

In these cases, by consideration of a threshold stress ( $\sigma_{th}$ ) [93], it is possible to use the pre-defined stress exponents [86,94,95]. This is especially the case for HEAs when the microstructure exhibited multi-phase characteristics during the process of hot deformation as a result of the interaction of dislocations with the second phase particles [62,84,95]. These particles might be present initially [95], or form at the hot working temperature, and/or precipitate during hot working [62,84]. For instance, for the SnAlZnCuMg alloy, Khodashenas et al. [95] obtained the values of  $n'$ ,  $\beta$ ,  $n$ , and  $Q$  as 15.085, 0.133, 11.471, and 110 kJ/mol, respectively. As a result,  $\alpha \approx \beta/n'$  was calculated as  $0.0088 \text{ MPa}^{-1}$ . It can be seen that, by consideration of the conventional method explained above, high values for  $n'$  and  $n$  are determined, which do not conform to the expected value of 5. To investigate the potential of using  $\sigma_{th}$ , Eq. (6) was rewritten as  $Z = A'(\sigma - \sigma_{th})^{n'}$ , which can be simplified as  $Z = A'(\sigma - \sigma_{th})^n$  and finally as follows:

$$Z^{(1/n')} = A'^{(1/n')} \sigma - A'^{(1/n')} \sigma_{th} \quad (16)$$

By temporary consideration of  $n'=5$  and based on the plot of  $Z^{(1/n')}$  versus  $\sigma$  (Fig. 19a), the value of  $\sigma_{th}$  can be obtained as the minus of the ratio of intercept/slope ( $318.21/4.3748 = 72.74 \text{ MPa}$ ). Now, the equation  $Z = A'(\sigma - \sigma_{th})^n$  can be changed as follows:

$$\ln Z = \ln A' + n' \ln(\sigma - \sigma_{th}) \quad (17)$$

Accordingly, the plot of  $\ln Z$  versus  $\ln(\sigma - \sigma_{th})$  in Fig. 19b can be used for obtaining the value of  $n'$  as 4.89. Eq. (8) can also be expressed as  $Z = A \{ \sinh \{ \alpha(\sigma - \sigma_{th}) \} \}^n$ , and finally as follows:

$$\ln Z = \ln A + n \ln \{ \sinh \{ \alpha(\sigma - \sigma_{th}) \} \} \quad (18)$$

Therefore, the plot of  $\ln Z$  versus  $\ln \{ \sinh \{ \alpha(\sigma - \sigma_{th}) \} \}$  in Fig. 19c can be used to obtain the value of  $n=4.96$ . It can be seen that both  $n'$  and  $n$  are close to 5 according to this modified analysis.

As another example, for the Al<sub>0.3</sub>CoCrFeNi alloy, Tong et al. [84] observed that the value of  $\sigma_{th}$  decreases with increasing the deformation temperature (Fig. 20), and hence, the barriers to overcome the precipitates decrease. This can be explained by the fact that the atoms are more likely to be activated and diffuse at elevated temperature, which is more conducive to the occurrence of dislocation climb [84]. In some cases, increasing the temperature might also be responsible for the disappearance of the secondary phases [62], which might play a role in this respect.

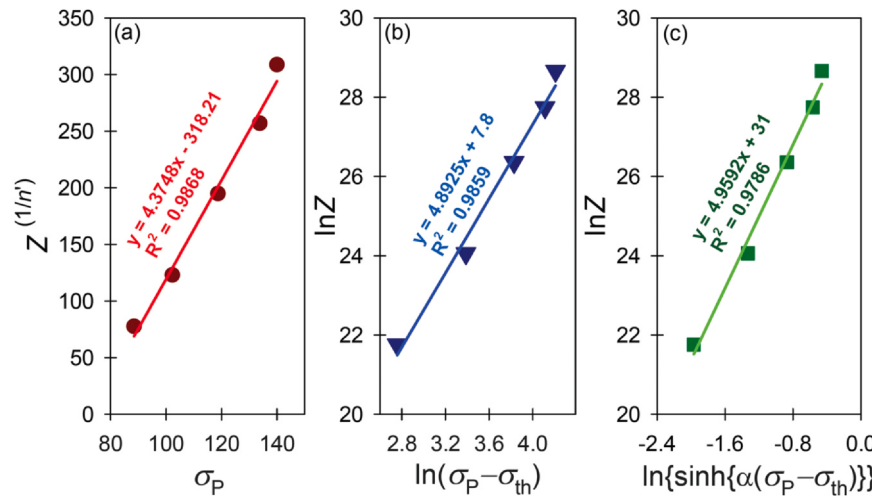


**Fig. 19.** Plots used for obtaining (a)  $\sigma_{th}$ , (b)  $n'$ , and (c)  $n$  [95]. Peak stress ( $\sigma_P$ ) and  $Z$  are expressed in MPa and  $s^{-1}$ , respectively.

## 5. Modeling and prediction of flow stress

The characterization of hot flow behavior is important for designing the metalforming processes, where proper constitutive relationships are often used to describe the flow behavior in computer codes to model the hot deformation response of the parts under the prevailing loading conditions [96–99]. Regarding the flow stress modeling of HEAs, there are few reports on the strain-compensated Arrhenius model [40,52–54,57,79,85,100], artificial neural network (ANN) model [85], Zerilli-Armstrong (ZA) model [100], Johnson-Cook (JC) model [100,101], and other models such as Hensel-Spittel equation [100] and dislocation density-based multiscale constitutive model [102].

### 5.1. Arrhenius model

In Section 4, based on  $Z = \dot{\varepsilon} \exp(Q/RT) = A \{ \sinh(\alpha\sigma) \}^n$ , the procedure to obtain the values of  $A$ ,  $n$ ,  $\alpha$ , and  $Q$  was presented. If the values of flow stress ( $\sigma$ ) for a given value of strain ( $\varepsilon$ ) at different deformation temperatures and strain rates are used for these calculations, the values of  $A$ ,  $n$ ,  $\alpha$ , and  $Q$  for that  $\varepsilon$  can be obtained [97]. This can be repeated for other strain values, and hence, the values of  $A$ ,  $n$ ,  $\alpha$ , and  $Q$  can be correlated with strain. This is known as strain compensation, and an example is shown in Fig. 21 for the hot compressed AlCrCuFeNi HEA [57]. By rearrangement of Eq. (8), the flow stress equation for a given  $\varepsilon$  can be expressed as follows:

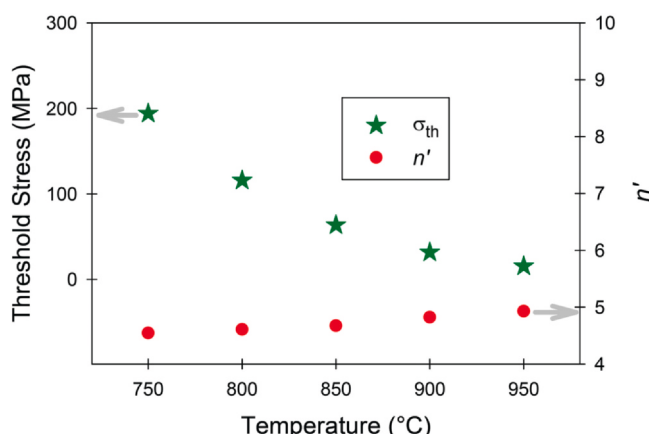


**Fig. 20.** Variation of  $\sigma_{th}$  and  $n'$  of  $\text{Al}_{0.3}\text{CoCrFeNi}$  HEA as a function of temperature [84].

$$\sigma = \frac{1}{\alpha} \left\{ \sinh^{-1} \left( \frac{Z}{A} \right)^{1/n} \right\} = \frac{1}{\alpha} \ln \left\{ \left( \frac{Z}{A} \right)^{1/n} + \sqrt{\left( \frac{Z}{A} \right)^{2/n} + 1} \right\}^{1/2}$$
(19)

In this way, the dependency of flow stress on  $Z$  (in fact the deformation temperature and strain rate) at each strain is obtained. Moreover, via the dependency of  $A$ ,  $n$ ,  $\alpha$ , and  $Q$  on the strain, Eq. (19) can also be used to relate the flow stress to strain. The applicability of this technique for the hot compressed AlCrCuFeNi HEA is shown in Fig. 22 [57].

The good capability of this model for predicting the flow stress can be seen in Fig. 22, which reveals its potentials. However, for improving its predictive ability, more reasonable utilization of the model according to the principles of the Arrhenius model, and practical simplification of the time-consuming calculations, a simplified approach has been proposed by Mirzadeh [103], and its potentials were subsequently verified by Rastegari et al. [104] and Shalbafi et al. [105]. In this approach, the values of  $\alpha$  and  $Q$  are obtained from the peak stress ( $\sigma_P$ ) analysis, and hence, they are considered independent of  $\varepsilon$ . It is noteworthy that the consideration of  $\sigma_P$  in the Arrhenius equation is a standard procedure for constitutive analysis. Afterward, the values of  $n$  and  $\ln A$  are considered as the strain-dependent parameters to account for the strain dependency of the flow stress. While the required calculations were significantly simplified, better prediction abilities for unseen deformation conditions were obtained by this approach. Therefore, the applicability of this simplified model for the flow stress prediction of HEAs needs to be evaluated.

The strain compensation technique can also be applied based on Eq. (15) for flow stress modeling [106–108], which is a promising approach for obtaining more reliable constitutive equations due to its physically-based nature. Accordingly, the evaluation of its applicability for hot deformed HEAs is worthy of investigation.

### 5.2. ANN model

For developing an ANN model, choosing specific relationships between inputs and outputs is not required, making its utilization straightforward. Moreover, this technique is very powerful in capturing the relationships between the variables. However, it is a black-box technique, where no account is taken of the physical relationships between inputs and outputs. Accordingly, a good database is required to construct the ANN model, and intrinsically, the use of the model for inputs outside the range used to construct the model is limited and should be applied with caution. For flow stress modeling, the inputs are temperature, strain, and the logarithm of

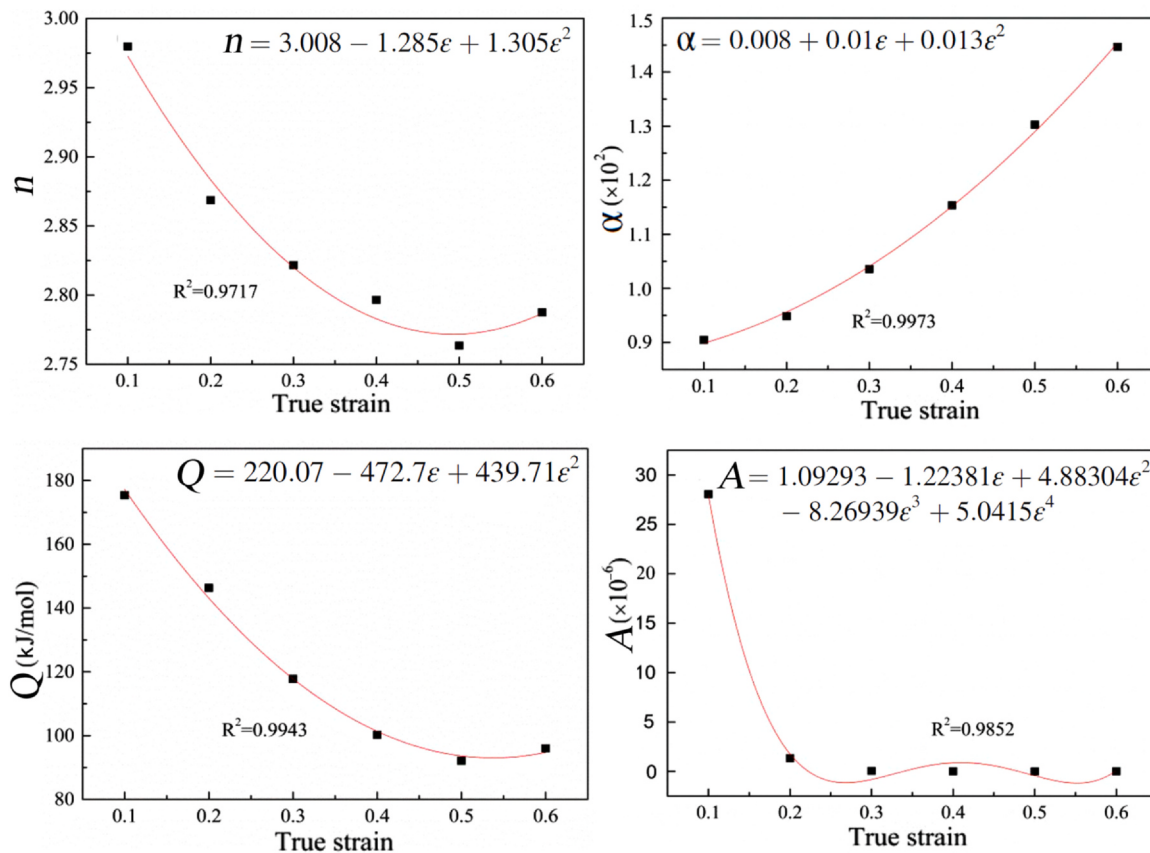


Fig. 21. Strain dependent  $A$ ,  $n$ ,  $\alpha$ , and  $Q$  for hot compressed AlCrCuFeNi HEA [57].

strain rate, while the output is the flow stress [109–111]. Pre-normalization of the input and output data is usually required. For this purpose, since the values of strain rate change by several orders of magnitude, the strain rate cannot be directly normalized due to the problem of too small values for low strain rates and non-uniform distribution of the normalized value. Accordingly, the logarithmic form of strain rate is usually considered [85,112–114]. For HEAs, the ANN technique has been applied for the flow stress modeling of (CoCrFeNi)<sub>90</sub>Zr<sub>10</sub> alloy by Jain et al. [85], where the schematic representation of the ANN model is shown in Fig. 23. The average absolute relative error (AARE) for the ANN model was obtained as 1.22%, which reveals the great potential of ANN for modeling and prediction of flow stress of HEAs. The use of this technique for HEAs is in its infancy and there is only one report [85], and hence, it is expected that this technique will be extensively used in future works.

### 5.3. Zerilli-Armstrong model

The Zerilli-Armstrong (ZA) model [115] has been developed based on thermally activated dislocation mechanics. The formula can be represented as follows for FCC metals:

$$\sigma = C_0 + C_2 \varepsilon^{0.5} \exp(-C_3 T + C_4 T \ln \dot{\varepsilon}) \quad (20)$$

where  $C_0$  and  $C_2$  have the unit of MPa and  $C_3$  and  $C_4$  have the unit of K<sup>-1</sup>. For better fit ability, it is possible to consider  $n$  instead of 0.5 [100,116]. There are many modifications for the Zerilli-Armstrong model for enhancing its predictive ability [116–121]. The most widely used one is based on the work of Samantaray et al. [117]:

$$\sigma = (C_1 + C_2 \varepsilon^n) \exp \{-(C_3 + C_4 \varepsilon)(T - T_r) + (C_5 + C_6(T - T_r)) \ln (\dot{\varepsilon}/\dot{\varepsilon}_r)\} \quad (21)$$

where  $\dot{\varepsilon}_r$  and  $T_r$  are the reference strain rate and reference temperature, respectively. This equation has a greater number of constants ( $C_1$ ,  $C_2$ ,  $C_3$ ,  $C_4$ ,  $C_5$ , and  $C_6$ ). This modified model considers the coupled effects of temperature, strain, and strain rate. The applicability of the original ZA and modified models are examined by Brown et al. [100] for CoCrFeMnNi HEA, and the results are shown in Fig. 24. It can be seen that both models give moderate fitting abilities, which has been ascribed to the applicability of ZA models for high strain rates [100]. However, the modified model has been successfully applied for other engineering alloys, and hence, more research works are needed to assess the applicability of this model for a broader range of HEAs.

### 5.4. Johnson-Cook model

By consideration of separate effects of  $\varepsilon$ ,  $\dot{\varepsilon}$ ,  $T$ , Johnson and Cook [122] proposed the following equation:

$$\sigma = (\sigma_{0r} + B \varepsilon^n) \times \left(1 + C \ln \frac{\dot{\varepsilon}}{\dot{\varepsilon}_r}\right) \times \left(1 - \left(\frac{T - T_r}{T_m - T_r}\right)^q\right) \quad (22)$$

where  $\dot{\varepsilon}_r$  and  $T_r$  are related to the considered reference condition (typically the lowest temperature and strain rate [107,123]). Moreover,  $B$ ,  $C$ , and  $q$  are material's constants. On the other hand,  $T_m$  is the melting point of the material. Furthermore,  $\sigma_{0r}$  is the yield stress at the considered reference condition, which can be obtained from the flow curve. At the reference condition,  $\sigma = \sigma_{0r} + B \varepsilon^n$  or  $\sigma - \sigma_{0r} = B \varepsilon^n$ , and hence, the following equation can be determined:

$$\ln(\sigma - \sigma_{0r}) = \ln B + n \ln \varepsilon \quad (23)$$

Therefore,  $n$  and  $\ln B$  can be obtained from the slope and intercept of the plot of  $\ln(\sigma - \sigma_{0r})$  against  $\ln \varepsilon$ , respectively. On the one hand, at  $T = T_r$ , we have

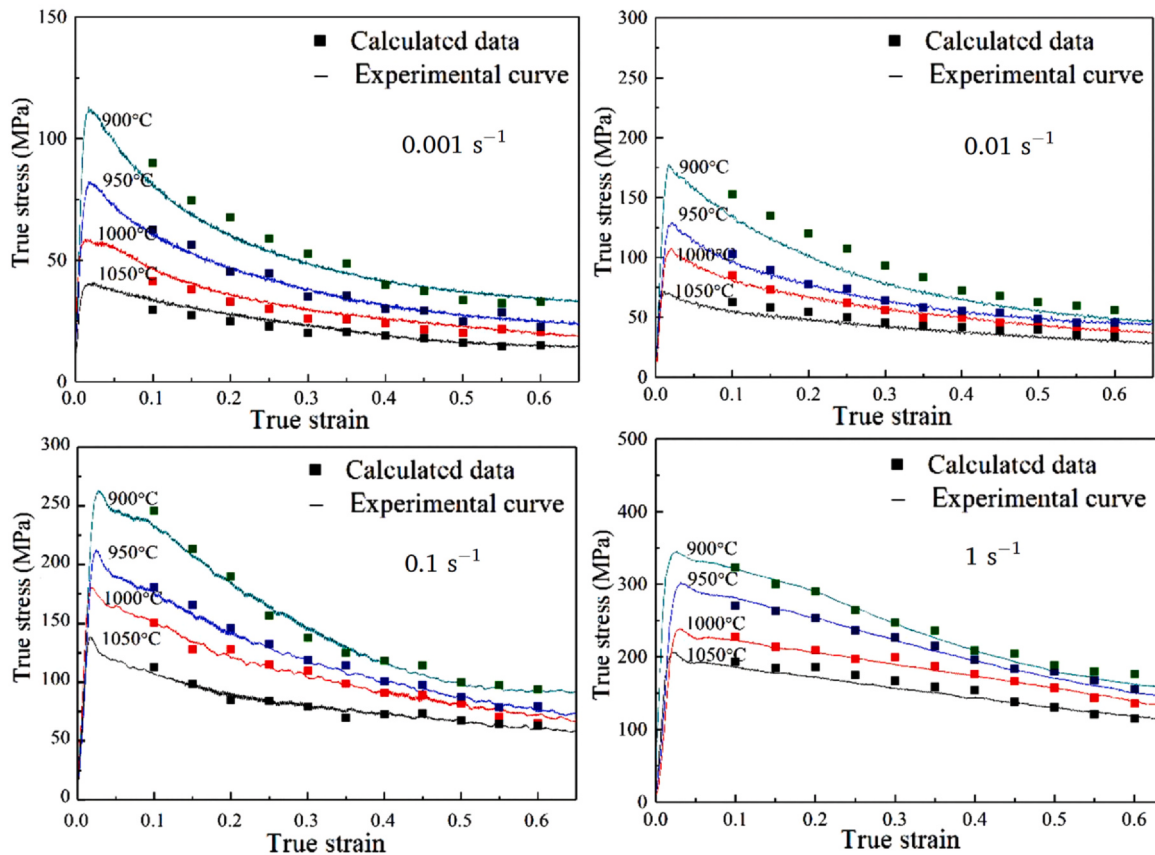


**Fig. 22.** Comparison of predicted and experimental flow stress values for hot compressed AlCrCuFeNi HEA [57].

$$\sigma/(\sigma_{0r} + Be^n) = 1 + C \ln (\dot{\varepsilon}/\dot{\varepsilon}_r) \quad (24)$$

Accordingly,  $C$  can be obtained from the slope of the plot of  $\sigma/(\sigma_{0r} + Be^n)$  vs.  $\ln(\dot{\varepsilon}/\dot{\varepsilon}_r)$  with an intercept of 1 at constant strains and various strain rates. On the other hand, at  $\dot{\varepsilon} = \dot{\varepsilon}_r$ , we have Eq. (25) and hence, Eq. (26):

$$1 - \sigma/(\sigma_{0r} + Be^n) = [(T - T_r)/(T_m - T)]^q \quad (25)$$

$$\ln[1 - \sigma/(\sigma_{0r} + Be^n)] = q \ln[(T - T_r)/(T_m - T)] \quad (26)$$

Therefore,  $q$  can be obtained from the slope of the plot of  $\ln[1 - \sigma/(\sigma_{0r} + Be^n)]$  versus  $\ln[(T - T_r)/(T_m - T)]$  with an intercept of 0 at constant strains and various temperatures. Therefore, the model can be constructed.

The original Johnson-Cook (JC) model suffers from the experimental observation of the dependency of  $C$  and  $q$  on the strain, while they should be constants. Accordingly, the separate consideration of  $\varepsilon$ ,  $\dot{\varepsilon}$ ,  $T$  effects seems inappropriate, and coupled effects of these variables should be considered. For this purpose, various modified Johnson-Cook models have been proposed [101,123–127]. Among these models, Lin et al. [125] proposed a promising modification for the JC model by consideration of additional constant of  $A_1$ ,  $B_1$ ,  $B_2$ ,  $C_1$ ,  $\lambda_1$ ,  $\lambda_2$ :

$$\sigma = (A_1 + B_1\varepsilon + B_2\varepsilon^2) \times \left(1 + C_1 \ln \frac{\dot{\varepsilon}}{\dot{\varepsilon}_r}\right) \times \exp\left(\left(\lambda_1 + \lambda_2 \ln \frac{\dot{\varepsilon}}{\dot{\varepsilon}_r}\right)(T - T_r)\right) \quad (27)$$

The JC model does not take into account the temperature rise from plastic work transformation. Given the adiabatic temperature rise converted by plastic deformation work upon dynamic loading, a modified JC model has been proposed by Zhang et al. [101] for

AlCoCr<sub>1.5</sub>Fe<sub>1.5</sub>NiTi<sub>0.5</sub> HEA with good predicting potential. For HEAs, the JC model has been used for flow stress modeling of CoCrFeMnNi alloy by Brown et al. [100] and AlCoCr<sub>1.5</sub>Fe<sub>1.5</sub>NiTi<sub>0.5</sub> alloy by Zhang et al. [101]. Based on the results of Brown et al. [100] shown in Fig. 25, the modified JC model has a good capability to model the flow stress of CoCrFeMnNi HEA, while the original JC model shows a significant deviation.

### 5.5. Hensel-Spittel model

Another useful equation for modeling and prediction of hot deformation flow stress has been proposed by Hensel and Spittel [128] as follows:

$$\sigma = Ae^{m_1 T} \varepsilon^{m_2} \dot{\varepsilon}^{m_3} e^{m_4/\varepsilon} (1 + \varepsilon)^{m_5 T} e^{m_6 \varepsilon} \dot{\varepsilon}^{m_7 T} T^{m_8} \quad (28)$$

where  $A$ ,  $m_1$ ,  $m_2$ ,  $m_3$ ,  $m_4$ ,  $m_5$ ,  $m_6$ ,  $m_7$ , and  $m_8$  are regression coefficients. This model is basically a combination of classical power law model of strain rate and Hollomon and Swift models with their material constants considered as functions of strain and temperature [129]. While there are many constants, this model needs modification regarding the strain rate sensitivity. Accordingly, Eq. (28) has been modified/simplified by Spigarelli and El Mehtedi [130] as follows for reducing the regression coefficients and better modeling ability:

$$\sinh(\alpha\sigma) = Ae^{m_1 T} \varepsilon^{m_2} \dot{\varepsilon}^{m_3} e^{m_4/\varepsilon} (1 + \varepsilon)^{m_5 T} e^{m_6 \varepsilon} \quad (29)$$

For HEAs, the original and modified Hensel-Spittel models have been used for flow stress modeling of CoCrFeMnNi alloy by Brown et al. [100]. It was shown that Eq. (29) has a better capability to model the flow stress of CoCrFeMnNi HEA compared to Eq. (28).

### 5.6. Dislocation density-based model

He et al. [102] proposed a dislocation density-based multiscale constitutive model to describe the hot deformation of HEAs. Their model is based on Fig. 26, which shows the typical hardening behaviors of HEAs at intermediate-temperatures and strain rates for uniaxial deformation. Stage I represents the first hardening section, where dislocation multiplication and accumulation dominate this stage. Both temperature and strain rate have significant effect on stage II with approximately constant work hardening rate. Strain rate has more pronounced impact on the length of this period, and temperature affects both duration and the hardening rate. Stage II may disappear at elevated temperatures and static or quasi-static strain rates. In stage III, with the accumulation of dislocations, DRV becomes stronger and recrystallization is locally activated caused by sustaining growth of stored energy. Hardening rate decreases markedly in this stage and continues to decrease until hardening, recovery and recrystallization reaching a relative balance state in stage IV. Then, the hardening rate decreases to zero. It was found that the proposed model can accurately describe different hardening stages of CoCrFeMnNiC<sub>0.5</sub> HEA under uniaxial deformation. However, the decrease of flow stress caused by DRX after reaching peak stress has not been considered in this model, which should be treated in future works.

For other engineering alloys, Lin and coworkers [131,132] have proposed unified dislocation density-based models according to the classical dislocation density-based model [133], which are based on  $\sigma = \sigma_y + \sigma_i$ , where  $\sigma$  is the flow stress,  $\sigma_y$  is the short-range stress component for activating dislocation motion, and  $\sigma_i$  is the dislocation interaction stress component expressed as follows:

$$\sigma_i = M\alpha Gb\sqrt{\rho_i} \quad (30)$$

Where  $M$ ,  $\alpha$ ,  $G$ ,  $b$ , and  $\rho_i$  represent Taylor factors (3.06 for FCC alloys), dislocation interaction constant (ranges from 0.2 to 0.8), the shear modulus (sensitive to deformation temperature), the magnitude of burgers vector, and the average dislocation density, respectively. Following Kocks-Meching (K-M) model, the changing rate of dislocation density is given by  $\dot{\rho}_i = \dot{\rho}_i^+ - \dot{\rho}_i^-$ , where  $\dot{\rho}_i^+$  and  $\dot{\rho}_i^-$  represent the changing rates of the dislocation density caused by work hardening and DRV, respectively. In this way, it is possible to propose a specific dislocation density-based model for the studied material. These kinds of models can be also applied to HEAs.

## 6. Discussion and future directions

A combination of cold/warm working and heat treatment for static recrystallization [134–136] is typically used for grain refinement of HEAs, where the grain size is generally on the order of several micrometers. An effective and industrially applicable method for microstructural refinement is hot deformation by utilization of DRX [20,23,34,137,138]. It was also demonstrated in this overview that the potential of DRX for grain refinement is superior to that of SRX for HEAs. The well-known effect of hot working in reducing the effects of defects is also significant, which might be important for the actual application of the HEAs, especially for the powder metallurgy parts (reduction of porosity level).

Another viable approach is the utilization of techniques with in-situ hot working such as FSP for the enhancement of microstructure and mechanical properties for HEAs. FSP applies SPD at elevated temperatures [139–141], which refines the grain size by DRX, leads to the fragmentation and dispersion of the secondary phase particles, and reduces the casting defects [27,142,143]. Therefore, the friction stir technology is expected to be extensively utilized in future works on HEAs.

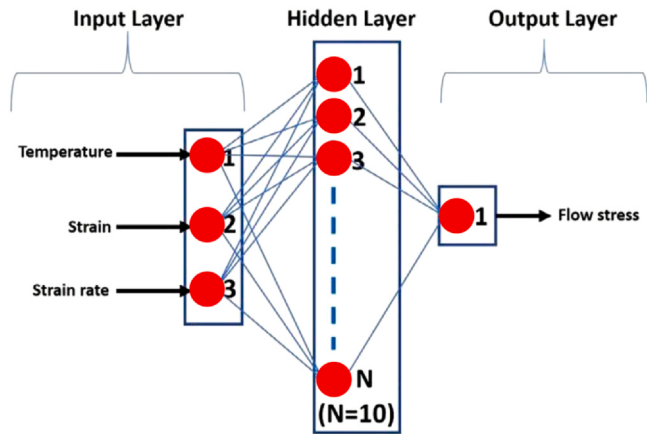


Fig. 23. Schematic representation of the ANN model used by Jain et al. [85].

Interestingly, the application of elevated-temperature thermo-mechanical processing and SPD for obtaining superplastic microstructures has been a subject of a few studies [29,31,144–149], where the utilization of thermomechanical processing (rolling + annealing), high-pressure torsion (HPT), multidirectional forging (MDF), high-ratio differential speed rolling (HRDSR), and FSP has been reported. Future studies might focus on other common processing techniques such as equal channel angular pressing (ECAP) for attaining high strain rate superplasticity [139]. Moreover, the SPD process variables might significantly affect the grain size, boundary misorientations, and dispersion and morphology of second phases, which need more investigations. On the other hand, systematic works on the actual superplastic forming of these alloys remains to be performed [11]. The thermal stability of the microstructure of HEAs and the formation/dissolution of phases at the superplastic temperature should be investigated for a wider range of HEAs. Special attention to the two-phase HEAs is also an important matter in future works. Phase transformations at the deformation temperature might promote superplastic behavior, and a better understanding of the accommodation processes and cavitation during superplastic flow will be useful. While the superplasticity of quasi-single phase FCC, dual-phase, or multi-phase HEAs has been studied so far, it is expected that the superplasticity of BCC HEAs, HCP HEAs, and MEAs gain considerable attentions in the near future.

Regarding the behavior of the HEAs at elevated-temperatures, it was shown that the deformation temperature greatly affects the mechanical properties of HEAs [150]. It can be concluded that at temperatures higher than  $\sim 0.4$ – $0.5T_m$ , the yield stress of HEAs drops suddenly, which can be related to the thermally activated dislocation glide, and if applicable, the decreased strength of secondary phases. In this respect, the effects of alloying element addition might be significant [33]. While the grain size dependency of the yield stress at low temperatures is significant, it becomes negligible at temperatures higher than  $0.5T_m$ , which is in accordance with the operation of the usual deformation mechanism in the hot working regime (the glide and climb of dislocations, i.e. dislocation creep), for which the dependency of flow stress on grain size is not significant [36,151–153]. Moreover, both DRX fraction and grain size might strongly depend on the doped elements such as C and N [53,54,154]. Accordingly, future works might be focused on the effect of alloying elements on the elevated-temperature properties and microstructural evolutions of HEAs.

As mentioned in the previous paragraph, DRX is one of the main restoration mechanisms during hot deformation of HEAs. In this respect, the propagation of DRX via the necklace mechanism has been observed for various HEAs, where the grain boundary bulging is responsible for the formation of fine grains in the necklace

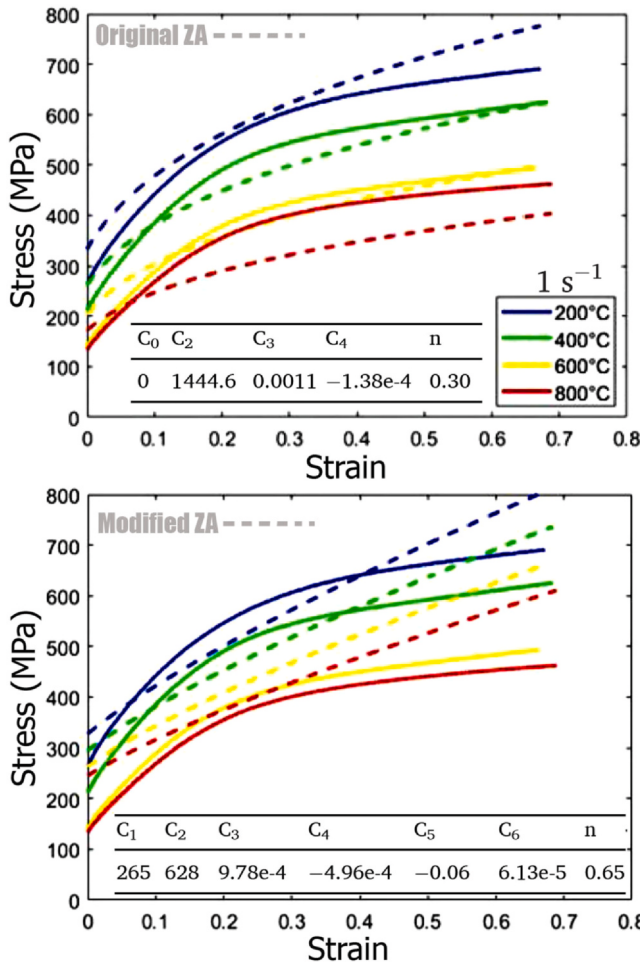


Fig. 24. Original and modified ZA models applied on CoCrFeMnNi HEA [100].

mechanism [45]. Moreover, the increase in the recrystallization fraction and DRX grain size by increasing the deformation temperature and decreasing strain rate (decreasing the Zener-Hollomon parameter) has also been noted [23,37,39–42]. The change in the DRX grain size with strain seems to be insignificant for HEAs, which is a characteristic feature of the necklace DRX mechanism (the growth of each grain stops by the concurrent deformation) [43,155–157]. However, the initial grain size and morphology might affect the hot deformation behavior and restoration mechanisms, where the single peak, multiple peak (cyclic), and the multiple transient steady state (MTSS) behaviors as the main types of DRX flow behavior are dependent on both Zener-Hollomon parameter and initial grain size [158–162]. For instance, the characteristic points such as critical, peak, and steady state strains are highly dependent on the grain size, and hence, at large grain sizes (e.g. for the as-cast condition), the steady state strain is high and might not be achieved during processing/testing. Therefore, the effect of the initial microstructure on the hot deformation behavior of HEAs is worthy of investigation. It is noteworthy that the eutectic HEAs show the most effective grain refinement during hot deformation, which could be attributed to the small initial grain size, PSN effect of the fragmented particles, and high localized deformation at the interfaces in the eutectic microstructure [41]. Accordingly, investigating the effect of the deformation conditions (Zener-Hollomon parameter and strain) and the presence of phases on the microstructural evolution and DRX behavior constitutes a major part of future works.

Due to the importance of DRX during hot deformation of HEAs, determination of the initiation point of DRX is of utmost

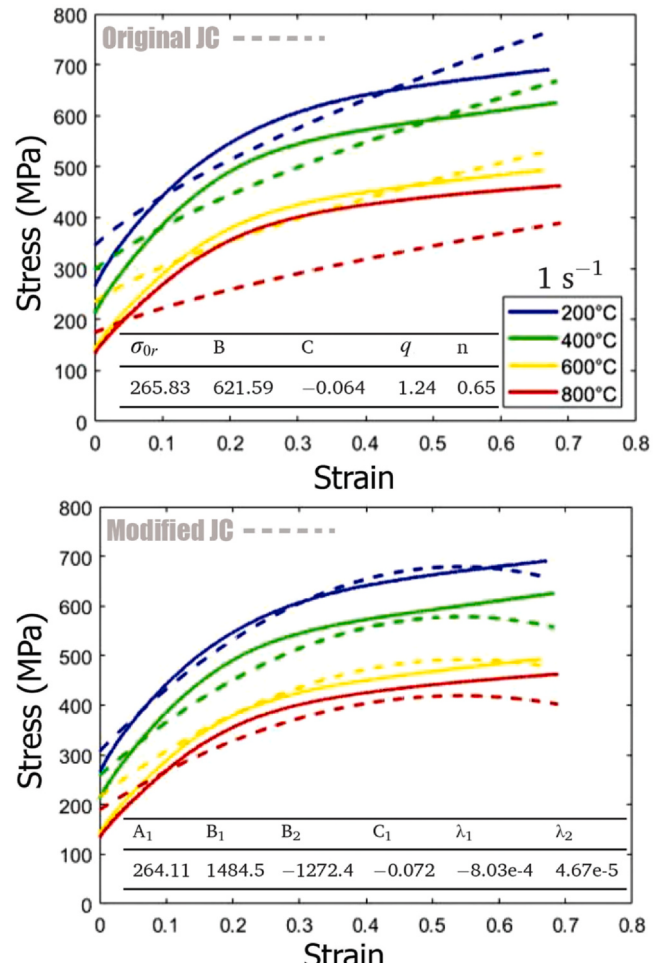


Fig. 25. Original and modified JC models applied to CoCrFeMnNi HEA [100].

importance. It should be noted that the shape of the flow curve at elevated temperatures might be similar to that of DRV behavior without the appearance of the clear peak point. However, work hardening rate analysis in conjunction with microstructural studies should be used to reveal the occurrence or absence of DRX. The inflection points in the plots of the work hardening rate ( $\theta = d\sigma/d\varepsilon$ ) versus  $\sigma$  can be used to obtain the critical stress for initiation of DRX ( $\sigma_c$ ) [163–165]. These inflection points are equivalent to a minimum on the plot of  $-d\theta/d\sigma$  versus  $\sigma$  [48,49]. The application of this important tool in hot working needs much more attention for HEAs, which should be also correlated to the results of microstructural investigations by EBSD and other techniques [166,167]. Dynamic precipitation might play a critical role in the inhibition of DRX [60,61]. For instance, for AlCoCrFeNi<sub>2.1</sub> eutectic HEA, at higher temperatures, DRX was the main mechanism for controlling the microstructural evolution. However, the dominant restoration mechanism at lower temperatures was identified as DRV due to the retardation effect of precipitates [60]. Accordingly, precipitation in highly alloyed HEAs might be an important factor in determining the hot deformation behavior [62,63]. Therefore, future works might focus on the controlling of precipitation for tailoring the elevated-temperature properties of HEAs.

Based on the above finding, construction of the processing maps is a prerequisite for the practical hot forming of HEAs. In this regard, it was also argued that flow softening behavior might occur due to the onset of flow instability and cracking, and hence, it might not be appropriate to investigate the hot working behavior only based on the shape of the flow curves [56]. Consequently, the investigation of

hot working behavior by constructing the processing maps will be an important part of future works. Moreover, the influence of state of stress (that is different in tension, compression, and torsion tests) on the processing map and instability regions might be important due to the fact that to achieve complete microstructure control in a component, the state of stress will have to be considered [168]. In the instability regimes, hot working might lead to cracking. However, in the regions with high power dissipation efficiencies, microstructural refinement by DRX might happen, and hence, these regions are safe ones for hot working [56–59,169–171].

Regarding the hot deformation behavior, the utilization of constitutive equations for the presentation of material flow has also been widely investigated for HEAs. Most of the works have focused on the hyperbolic sine law, and a few works are based on the power law. However, the majority of the works only considered the apparent values of  $n$  and  $Q$ , and hence, the comparison of the obtained values with the pre-defined values from the creep theories needs much more attention [39,76,89–92]. Another important progress in the constitutive analysis is the consideration of temperature-dependent Young's modulus and shear modulus as well as diffusivity, which makes the analysis more physically-based [39,76,89–92]. More importantly, due to the presence of phases or their precipitation during hot working, a  $\sigma_{th}$  might arise. For instance, it has been reported that  $\sigma_{th}$  is also temperature-dependent. The threshold stress has been considered in a few works [62,84,95], and hence, it needs much more attention.

Despite the importance of flow curve modeling for industrial applications, few works on hot working of HEAs are focused on this aspect. Regarding the flow stress modeling of HEAs, there are few reports on the strain-compensated Arrhenius model, artificial neural network (ANN) model, Zerilli-Armstrong (ZA) model, Johnson-Cook (JC) model, Hensel-Spittel model, and dislocation density-based multiscale constitutive model. Regarding the strain-compensated Arrhenius model, the developed simplified approach with better predictive ability, more reasonable utilization of the model according to the principles of the Arrhenius model, and effective simplification of the time-consuming calculations can be considered in future works [103], in which the values of  $\alpha$  and  $Q$  are obtained from the peak stress ( $\sigma_p$ ) analysis, and hence, they are considered to be independent of  $\epsilon$ . Moreover, the strain compensation technique can also be applied by the consideration of temperature-dependent Young's modulus and shear modulus as well as diffusivity [172,173], which is a promising approach for obtaining more reliable constitutive equations due to its physically-based nature. On the other hand, the use of ANN for flow stress prediction of HEAs is in its infancy, and hence, it is expected that this technique is extensively used in future works. Promising models such as the modified Zerilli-

Armstrong model [117] and modified Johnson-Cook model [125] have not been extensively utilized for flow stress modeling of HEAs, and much more attention is required. The famous DRX/DRV model, based on the consideration of saturation stress for DRV and Johnson-Mehl-Avrami-Kolmogorov (JMAK) analysis for DRX [174–179], has not been considered for HEAs yet. Moreover, other promising constitutive models [180–183] can also be considered for flow stress modeling of HEAs.

Finally, the application of simulation techniques for hot working of HEAs needs to be evaluated [37,70]. Moreover, for the characterization of hot working behavior, the hot compression and hot tension tests have been used so far, where the implementation of the promising hot torsion test with the possibility to achieve much higher strains is worthy of investigation [184,185]. Finally, due to the capability of the additive manufacturing processes to produce the complex and industrially important parts, and the need for post-processing thermomechanical treatments in some cases [186–188], the investigation of the hot deformation behavior of additive manufactured HEAs has been started [189,190]. These subjects are expected to be widely investigated in the near future.

Based on this review paper, it was revealed that the basics of hot deformation behavior of HEAs are similar to other metallic materials in terms of flow behavior, restoration processes, features of processing maps, and constitutive analysis. However, due to the complexity of the chemical composition, sluggish diffusion might affect the flow behavior. In fact, the physical properties of HEAs are controlled to a large extent by the average of the properties of the constituting elements, which is different when compared to the conventional alloys with one principal element. More importantly, there is a possibility for precipitation/phase transformation due to exposure to the elevated temperature and/or the effect of hot deformation, which might significantly affect the flow behavior and restoration processes.

## 7. Summary

The hot deformation behavior and constitutive models to predict flow stress of high-entropy alloys were summarized in this work. The outcome of this overview can be summarized as follows.

- (1) It was discussed that hot deformation by utilization of DRX is an effective and industrially applicable method for microstructural refinement of HEAs, where its potential for grain refinement is superior to that of SRX for HEAs. The well-known effect of hot working in reducing the effects of defects is also significant, which might be important for the actual application of the HEAs. Another viable approach is the utilization of techniques with in-situ hot working such as FSP for the enhancement of microstructure and mechanical properties of HEAs.
- (2) It was shown that the deformation temperature greatly affects the mechanical properties of HEAs, especially at temperatures higher than  $\sim 0.4\text{--}0.5T_m$ . In this respect, the propagation of DRX via the necklace mechanism and the effect of deformation conditions on the DRX fraction and grain size were discussed for various HEAs. It was also noted that the work hardening rate analysis in conjunction with microstructural studies should be used to reveal the occurrence or absence of DRX for HEAs. Moreover, it was concluded that precipitation in highly alloyed HEAs might be an important factor in determining the hot deformation behavior of HEAs.
- (3) Construction of the processing maps to obtain the safe processing window was indicated as a prerequisite for the practical hot forming of HEAs. In this regard, it was also argued that flow softening behavior might occur due to the onset of flow instability and cracking, and hence, it might not be appropriate to

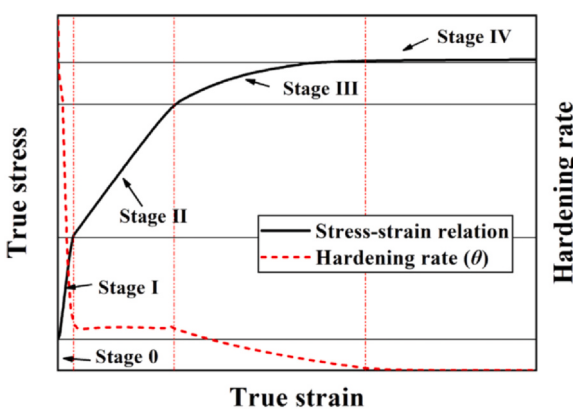


**Fig. 26.** Stage division of a typical stress-strain relation of HEAs [102].

- investigate the hot working behavior only based on the shape of the flow curves.
- (4) Utilization of constitutive equations for the presentation of material flow was summarized for HEAs. The consideration of the apparent values of  $n$  and  $Q$  was the usual practice. However, the consideration of temperature-dependent Young's modulus and shear modulus as well as diffusivity for physically-based analysis was also discussed. More notably, this approach necessitated the application of a threshold stress for obtaining material's constants that are consistent with the creep theories, which is especially the case at the presence of phases or their precipitation during hot working.
- (5) The reported works on constitutive modeling during hot deformation of HEAs were summarized as successful attempts for modeling of flow curves. However, it was revealed that the simplification of constitutive analysis and more attention to the physically-based nature of the used equations for obtaining more reliable constitutive equations are required. Moreover, the use of ANN for flow stress prediction of HEAs is in its infancy; while the modified Zerilli-Armstrong and Johnson-Cook models as well as the famous DRX/DRV model have not been extensively utilized for flow stress modeling of HEAs.

## Funding body

This work received no funding.

## Data Availability

The authors stated that the processed data required to reproduce these findings were available in this manuscript.

## Declaration of Competing Interest

The authors declare that they have no known competing financial interests or personal relationships that could have appeared to influence the work reported in this paper.

## References

- [1] J.W. Yeh, S.K. Chen, S.J. Lin, J.Y. Gan, T.S. Chin, T.T. Shun, C.H. Tsau, S.Y. Chang, Nanostructured high-entropy alloys with multiple principal elements: novel alloy design concepts and outcomes, *Adv. Eng. Mater.* 6 (5) (2004) 299–303.
- [2] P. Cantor, I.T.H. Chang, P. Knight, A.J.B. Vincent, Microstructural development in equiatomic multicomponent alloys, *Mater. Sci. Eng. A* 375 (2004) 213–218.
- [3] D.B. Miracle, O.N. Senkov, A critical review of high entropy alloys and related concepts, *Acta Mater.* 122 (2017) 448–511.
- [4] W. Li, D. Xie, D. Li, Y. Zhang, Y. Gao, P.K. Liaw, Mechanical behavior of high-entropy alloys, *Prog. Mater. Sci.* 118 (2021) 100777.
- [5] M. Asadiyi, Y. Zhang, L. Wang, D. Apelian, Y. Zhong, Design of ternary high-entropy aluminum alloys (HEAls), *J. Alloy. Compd.* 891 (2022) 161836.
- [6] Z. Li, S. Zhao, R.O. Ritchie, M.A. Meyers, Mechanical properties of high-entropy alloys with emphasis on face-centered cubic alloys, *Prog. Mater. Sci.* 102 (2019) 296–345.
- [7] S. Daryoush, H. Mirzadeh, A. Ataie, Amorphization, mechano-crystallization, and crystallization kinetics of mechanically alloyed AlFeCuZnTi high-entropy alloys, *Mater. Lett.* 307 (2022) 131098.
- [8] J. Chen, X. Zhou, W. Wang, B. Liu, Y. Lv, W. Yang, D. Xu, Y. Liu, A review on fundamental of high entropy alloys with promising high-temperature properties, *J. Alloy. Compd.* 760 (2018) 15–30.
- [9] P. Sathiyamoorthi, H.S. Kim, High-entropy alloys with heterogeneous microstructure: processing and mechanical properties, *Prog. Mater. Sci.* 123 (2022) 100709.
- [10] T.E. Whitfield, E.J. Pickering, L.R. Owen, O.N. Senkov, D.B. Miracle, H.J. Stone, N.G. Jones, An assessment of the thermal stability of refractory high entropy superalloys, *J. Alloy. Compd.* 857 (2021) 157583.
- [11] R. Motallebi, Z. Savaedi, H. Mirzadeh, Superplasticity of high-entropy alloys: a review, *Arch. Civ. Mech. Eng.* 22 (2022) 20.
- [12] M. Pole, M. Sadeghilardjani, J. Shittu, A. Ayyagari, S. Mukherjee, High temperature wear behavior of refractory high entropy alloys based on 4–5–6 elemental palette, *J. Alloy. Compd.* 843 (2020) 156004.
- [13] Y. Fu, J. Li, H. Luo, C. Du, X. Li, Recent advances on environmental corrosion behavior and mechanism of high-entropy alloys, *J. Mater. Sci. Technol.* 80 (2021) 217–233.
- [14] X. Yan, Y. Zhang, Functional properties and promising applications of high entropy alloys, *Scr. Mater.* 187 (2020) 188–193.
- [15] R. Hu, S. Jin, G. Sha, Application of atom probe tomography in understanding high entropy alloys: 3D local chemical compositions in atomic scale analysis, *Prog. Mater. Sci.* 123 (2022) 100854.
- [16] G.D. Sathiaraj, A. Pukenas, W. Skrotzki, Texture formation in face-centered cubic high-entropy alloys, *J. Alloy. Compd.* 826 (2020) 154183.
- [17] P. Yang, C. Liu, Q. Guo, Y. Liu, Variation of activation energy determined by a modified Arrhenius approach: roles of dynamic recrystallization on the hot deformation of Ni-based superalloy, *J. Mater. Sci. Technol.* 72 (2021) 162–171.
- [18] H. Zhu, H. Ou, Constitutive modelling of hot deformation behaviour of metallic materials, *Mater. Sci. Eng. A* (2021) 142473.
- [19] M. Annasamy, N. Haghdi, A. Taylor, P. Hodgson, D. Fabijanic, Dynamic recrystallization behaviour of AlxCoCrFeNi high entropy alloys during high-temperature plane strain compression, *Mater. Sci. Eng. A* 745 (2019) 90–106.
- [20] K. Edalati, H.W. Li, A. Kilmametov, R. Floriano, C. Borchers, High-pressure torsion for synthesis of high-entropy alloys, *Metals* 11 (8) (2021) 1263.
- [21] S. Picak, H.C. Yilmaz, I. Karaman, Simultaneous deformation twinning and martensitic transformation in CoCrFeMnNi high entropy alloy at high temperatures, *Scr. Mater.* 202 (2021) 113995.
- [22] S. Picak, T. Wegener, S.V. Sajadifar, C. Sobrero, J. Richter, H. Kim, T. Niendorf, I. Karaman, On the low-cycle fatigue response of CoCrNiFeMn high entropy alloy with ultra-fine grain structure, *Acta Mater.* 205 (2021) 116540.
- [23] R.R. Eleti, T. Bhattacharjee, L. Zhao, P.P. Bhattacharjee, N. Tsuji, Hot deformation behavior of CoCrFeMnNi FCC high entropy alloy, *Mater. Chem. Phys.* 210 (2018) 176–186.
- [24] Z. Li, Interstitial equiatomic CoCrFeMnNi high-entropy alloys: carbon content, microstructure, and compositional homogeneity effects on deformation behavior, *Acta Mater.* 164 (2019) 400–412.
- [25] M. Wu, C. Yang, M. Kuijer, I. Baker, Enhanced mechanical properties of carbon-doped FeNiMnAlCr high entropy alloy via hot-rolling, *Mater. Charact.* 158 (2019) 109983.
- [26] J. Zhou, H. Liao, H. Chen, A. Huang, Effects of hot-forging and subsequent annealing on microstructure and mechanical behaviors of Fe35Ni35Cr20Mn10 high-entropy alloy, *Mater. Charact.* (2021) 111251.
- [27] N. Kumar, M. Komarasamy, P. Nelaturu, Z. Tang, P.K. Liaw, R.S. Mishra, Friction stir processing of a high entropy alloy Al 0.1 CoCrFeNi, *JOM* 67 (5) (2015) 1007–1013.
- [28] Y. Cao, Y. Liu, B. Liu, W. Zhang, Precipitation behavior during hot deformation of powder metallurgy Ti-Nb-Ta-Zr-Al high entropy alloys, *Intermetallics* 100 (2018) 95–103.
- [29] P. Asghari-Rad, N.T.C. Nguyen, A. Zargaran, P. Sathiyamoorthi, H.S. Kim, Deformation-induced grain boundary segregation mediated high-strain rate superplasticity in medium entropy alloy, *Scr. Mater.* 207 (2022) 114239.
- [30] M. Kawasaki, T.G. Langdon, The contribution of severe plastic deformation to research on superplasticity, *Mater. Trans.* 60 (7) (2019) 1123–1130.
- [31] D.G. Shaysultanov, N.D. Stepanov, A.V. Kuznetsov, G.A. Salishchev, O.N. Senkov, Phase composition and superplastic behavior of a wrought AlCoCrCuFeNi high-entropy alloy, *JOM* 65 (12) (2013) 1815–1828.
- [32] R.B. Figueiredo, T.G. Langdon, Strategies for achieving high strain rate superplasticity in magnesium alloys processed by equal-channel angular pressing, *Scr. Mater.* 61 (1) (2009) 84–87.
- [33] L. Lin, X. Xian, Z. Zhong, C. Chen, Z. Zhu, Y. Wu, P.K. Liaw, A multi-phase CrMnFeCoNiAl0.75 high-entropy alloy with high strength at intermediate temperature, *Intermetallics* 120 (2020) 106744.
- [34] M.J. Jang, S. Praveen, H.J. Sung, J.W. Bae, J. Moon, H.S. Kim, High-temperature tensile deformation behavior of hot rolled CrMnFeCoNi high-entropy alloy, *J. Alloy. Compd.* 730 (2018) 242–248.
- [35] F. Otto, A. Dlouhy, C. Somsen, H. Bei, G. Eggeler, E.P. George, The influences of temperature and microstructure on the tensile properties of a CoCrFeMnNi high-entropy alloy, *Acta Mater.* 61 (15) (2013) 5743–5755.
- [36] M.H. Barezban, H. Mirzadeh, R. Roumina, R. Mahmudi, Constitutive analysis of wrought Mg-Gd magnesium alloys during hot compression at elevated temperatures, *J. Alloy. Compd.* 791 (2019) 1200–1206.
- [37] N.D. Stepanov, D.G. Shaysultanov, N.Y. Yurchenko, S.V. Zherebtsov, A.N. Ladygin, G.A. Salishchev, M.A. Tikhonovsky, High temperature deformation behavior and dynamic recrystallization in CoCrFeNiMn high entropy alloy, *Mater. Sci. Eng.: A* 636 (2015) 188–195.
- [38] M.J. Luton, C.M. Sellars, Dynamic recrystallization in nickel and nickel-iron alloys during high temperature deformation, *Acta Metall.* 17 (8) (1969) 1033–1043.
- [39] H.T. Jeong, H.K. Park, K. Park, T.W. Na, W.J. Kim, High-temperature deformation mechanisms and processing maps of equiatomic CoCrFeMnNi high-entropy alloy, *Mater. Sci. Eng. A* 756 (2019) 528–537.
- [40] M. Patnamsetty, A. Saastamoinen, M.C. Soman, P. Peura, Constitutive modelling of hot deformation behaviour of a CoCrFeMnNi high-entropy alloy, *Sci. Technol. Adv. Mater.* 21 (1) (2020) 43–55.
- [41] H.T. Jeong, H.K. Park, W.J. Kim, Dynamic recrystallization and hot deformation mechanisms of a eutectic Al0.7CoCrFeMnNi high-entropy alloy, *J. Alloy. Compd.* 871 (2021) 159488.
- [42] Q. Wang, T. Gao, H. Du, Q. Hu, Q. Chen, Z. Fan, L. Zeng, X. Liu, Hot compression behaviors and microstructure evolutions of a cast dual-phase NiCoFeCrAl0.7 high-entropy alloy, *Intermetallics* 138 (2021) 107314.
- [43] H. Mirzadeh, M. Roostaei, M.H. Parsa, R. Mahmudi, Dynamic recrystallization kinetics in Mg-3Gd-1Zn magnesium alloy during hot deformation, *Int. J. Mater. Res.* 107 (3) (2016) 277–279.

- [44] R.R. Eleti, A.H. Chokshi, A. Shibata, N. Tsuji, Unique high-temperature deformation dominated by grain boundary sliding in heterogeneous necklace structure formed by dynamic recrystallization in HfNbTaTiZr BCC refractory high entropy alloy, *Acta Mater.* 183 (2020) 64–77.
- [45] Q. Liu, G. Wang, Y. Liu, X. Sui, Y. Chen, S. Luo, Hot deformation behaviors of an ultrafine-grained MoNbTaTiV refractory high-entropy alloy fabricated by powder metallurgy, *Mater. Sci. Eng. A* 809 (2021) 140922.
- [46] L. Xu, Z. Chen, Y. Zheng, X. Wang, S. Han, S. Xiao, Y. Chen, Deformation behavior and microstructure evolution of as-cast Ti2ZrMo0.5Nb0.5 high entropy alloy, *J. Mater. Res. Technol.* (2021).
- [47] H.K. Zhang, H. Xiao, X.W. Fang, Q. Zhang, R.E. Logé, K. Huang, A critical assessment of experimental investigation of dynamic recrystallization of metallic materials, *Mater. Des.* 193 (2020) 108873.
- [48] E.I. Poliak, J.J. Jonas, A one-parameter approach to determining the critical conditions for the initiation of dynamic recrystallization, *Acta Mater.* 44 (1) (1996) 127–136.
- [49] G. Varela-Castro, J.M. Cabrera, J.M. Prado, Critical strain for dynamic recrystallization: The particular case of steels, *Metals* 10 (1) (2020) 135.
- [50] M. Kahnooji, A. Zarei-Hanzaki, H.R. Abedi, M. Hassanpour-Esfahani, M.S. Jalali, J. Gubicza, A. Heczel, An investigation into the dynamic recrystallization behavior of a non-equiautomic high entropy alloy, *Mater. Sci. Eng. A* 768 (2019) 138423.
- [51] F. Alijani, M. Reihanian, K. Gheisari, H. Miyamoto, Microstructure and high-temperature deformation behavior of FeCoNiMnV high entropy alloy, *Mater. Chem. Phys.* 256 (2020) 123675.
- [52] S.A. Sajadi, M.R. Toroghinejad, A. Rezaeian, G.R. Ebrahimi, A study of hot compression behavior of an as-cast FeCrCuNi2Mn2 high-entropy alloy, *J. Alloy. Compd.* (2021) 162732.
- [53] H. Yi, Y. Zhang, R. Xie, M. Bi, D. Wei, High-temperature deformation behaviors of the C-doped and N-doped high entropy alloys, *Metals* 11 (10) (2021) 1517.
- [54] J. Wang, Y. Liu, B. Liu, Y. Wang, Y. Cao, T. Li, R. Zhou, Flow behavior and microstructures of powder metallurgical CrFeCoNiMo0.2 high entropy alloy during high temperature deformation, *Mater. Sci. Eng. A* 689 (2017) 233–242.
- [55] K. Tang, L.B. Chen, S. Wang, R. Wei, Z.Y. Yang, F. Jiang, J. Sun, Development of a large size FCC high-entropy alloy with excellent mechanical properties, *Mater. Sci. Eng. A* 761 (2019) 138039.
- [56] M. Patnamsetty, M.C. Somani, S. Ghosh, S. Ahmed, P. Peura, Processing map for controlling microstructure and unravelling various deformation mechanisms during hot working of CoCrFeMnNi high entropy alloy, *Mater. Sci. Eng. A* 793 (2020) 139840.
- [57] X. Wang, Y. Zhang, X. Ma, High temperature deformation and dynamic recrystallization behavior of AlCrCuFeNi high entropy alloy, *Mater. Sci. Eng.: A* 778 (2020) 139077.
- [58] J. Jiang, M. Huang, Y. Wang, G. Xiao, Y. Liu, Y. Zhang, Unique hot deformation behavior and microstructure evolution of a dual FCC-phase CoCrCu1.2FeNi high entropy alloy, *J. Alloy. Compd.* 876 (2021) 160102.
- [59] N. Prasad, N. Bibhanshu, N. Nayak, G.S. Avadhan, S. Suwas, Hot deformation behavior of the high-entropy alloy CoCuFeMnNi, *J. Mater. Res.* 34 (5) (2019) 744–755.
- [60] M. Zaid Ahmed, K. Chadha, S.R. Reddy, D. Shahriari, P.P. Bhattacharjee, M. Jahazi, Influence of process parameters on microstructure evolution during hot deformation of Eutectic High-Entropy Alloy (EHEA), *Metall. Mater. Trans. A* 51 (12) (2020) 6406–6420.
- [61] Y. Zhang, X. Wang, J. Li, Y. Huang, Y. Lu, X. Sun, Deformation mechanism during high-temperature tensile test in an eutectic high-entropy alloy AlCoCrFeNi2.1, *Mater. Sci. Eng. A* 724 (2018) 148–155.
- [62] Q. Tian, G. Zhang, K. Yin, L. Wang, W. Wang, W. Cheng, Y. Wang, J.C. Huang, High temperature deformation mechanism and microstructural evolution of relatively lightweight AlCoCrFeNi high entropy alloy, *Intermetallics* 119 (2020) 106707.
- [63] K.S. Lee, J.H. Kang, K.R. Lim, Y.S. Na, Influence of compressive strain on the microstructural evolution of an AlCoCrFeNi high entropy alloy, *Mater. Charact.* 132 (2017) 162–168.
- [64] N. Haghdi, S. Primig, M. Annasamy, P. Cizek, P.D. Hodgson, D.M. Fabijanic, Dynamic recrystallization in AlXCoCrFeNi duplex high entropy alloys, *J. Alloy. Compd.* 830 (2020) 154720.
- [65] C. Zener, J.H. Hollomon, Effect of strain rate upon plastic flow of steel, *J. Appl. Phys.* 15 (1) (1944) 22–32.
- [66] H.J. McQueen, N.D. Ryan, Constitutive analysis in hot working, *Mater. Sci. Eng. A* 322 (1–2) (2002) 43–63.
- [67] J.J. Jonas, C.M. Sellars, W.M. Tegart, Strength and structure under hot-working conditions, *Metall. Rev.* 14 (1) (1969) 1–24.
- [68] H. Mirzadeh, Constitutive analysis of Mg-Al-Zn magnesium alloys during hot deformation, *Mech. Mater.* 77 (2014) 80–85.
- [69] C. Phaniraj, D. Samantaray, S. Mandal, A.K. Bhaduri, A new relationship between the stress multipliers of Garofalo equation for constitutive analysis of hot deformation in modified 9Cr-1Mo (P91) steel, *Mater. Sci. Eng. A* 528 (18) (2011) 6066–6071.
- [70] R. Jain, M.R. Rahul, S. Samal, V. Kumar, G. Phanikumar, Hot workability of Co-Fe-Mn-Ni-Ti eutectic high entropy alloy, *J. Alloy. Compd.* 822 (2020) 153609.
- [71] Z.C. Bai, X.F. Ding, Q. Hu, M. Yang, Z.T. Fan, X.W. Liu, Unique deformation behavior and microstructure evolution in high-temperature processing of a low-density TiAlVNb2 refractory high-entropy alloy, *J. Alloy. Compd.* 885 (2021) 160962.
- [72] T.G. Langdon, Identifying creep mechanisms in plastic flow, *Z. Metallkd.* 96 (2005) 522–531.
- [73] A.K. Mukherjee, An examination of the constitutive equation for elevated temperature plasticity, *Mater. Sci. Eng. A* 322 (1–2) (2002) 1–22.
- [74] H. Mirzadeh, J.M. Cabrera, A. Najafizadeh, Constitutive relationships for hot deformation of austenite, *Acta Mater.* 59 (16) (2011) 6441–6448.
- [75] W.F. Gale, T.C. Totemeier, Smithells Metals Reference Book, eighth ed., Elsevier, 2004.
- [76] J.Y. He, C. Zhu, D.Q. Zhou, W.H. Liu, T.G. Nieh, Z.P. Lu, Steady state flow of the FeCoNiCrMn high entropy alloy at elevated temperatures, *Intermetallics* 55 (2014) 9–14.
- [77] W. Steurer, Single-phase high-entropy alloys—a critical update, *Mater. Charact.* 162 (2020) 110179.
- [78] A. Li, Z. Huang, H. Xu, S. Wei, Effects of C and La on the tensile property and hot working characteristics of CoCrFeMnNi high-entropy alloy, *J. Phys. Conf. Ser.* 1622 (No. 1) (2020) 012024.
- [79] Y. Wang, J. Li, Y. Xin, C. Li, Y. Cheng, X. Chen, M. Rashad, Y. Liu, Effect of Zener-Hollomon parameter on hot deformation behavior of CoCrFeMnNiCo.5 high entropy alloy, *Alloy. Mater. Sci. Eng. A* 768 (2019) 138483.
- [80] H. Kaypour, S. Nategh, R. Gholamipour, A.R. Khodabandeh, High-temperature compressive behavior and kinetic analysis of Al0.4MnCrCoFeNi high entropy alloy, *Mater. Res. Express* (2021).
- [81] N. Shah, M.R. Rahul, S. Bysakh, G. Phanikumar, Microstructure stability during high temperature deformation of CoCrFeNiTa eutectic high entropy alloy through nano-scale precipitation, *Mater. Sci. Eng. A* 824 (2021) 141793.
- [82] F. Dong, Y. Yuan, W. Li, Y. Zhang, P.K. Liaw, X. Yuan, H. Huang, Hot deformation behavior and processing maps of an equiautomic MoNbHfZrTi refractory high entropy alloy, *Intermetallics* 126 (2020) 106921.
- [83] Y. Zhang, J. Li, J. Wang, S. Niu, H. Kou, Hot deformation behavior of as-cast and Homogenized Al0.5CoCrFeNi high entropy alloys, *Metals* 6 (11) (2016) 277.
- [84] Y. Tong, J.C. Qiao, Y. Yao, The constitutive model and threshold stress for characterizing the deformation mechanism of Al0.3CoCrFeNi high entropy alloy, *Mater. Sci. Eng.: A* 730 (2018) 137–146.
- [85] R. Jain, A. Jain, M.R. Rahul, A. Kumar, M. Dubey, R.K. Sabat, S. Samal, G. Phanikumar, Development of ultrahigh strength novel Co-Cr-Fe-Ni-Zr quasi-peritectic high entropy alloy by an integrated approach using experiment and simulation, *Materialia* 14 (2020) 100896.
- [86] J.M. Cabrera, A. Al Omar, J.M. Prado, J.J. Jonas, Modeling the flow behavior of a medium carbon microalloyed steel under hot working conditions, *Metall. Mater. Trans. A* 28 (11) (1997) 2233–2244.
- [87] H. Mirzadeh, Constitutive description of 7075 aluminum alloy during hot deformation by apparent and physically-based approaches, *J. Mater. Eng. Perform.* 24 (3) (2015) 1095–1099.
- [88] H. Mirzadeh, A comparative study on the hot flow stress of Mg-Al-Zn magnesium alloys using a simple physically-based approach, *J. Magnes. Alloy. 2* (3) (2014) 225–229.
- [89] H.T. Jeong, H.K. Park, H.S. Kang, W.J. Kim, Operation of solute-drag creep in an AlCoCrFeMnNi high-entropy alloy and enhanced hot workability, *J. Alloy. Compd.* 824 (2020) 153829.
- [90] W.J. Kim, H.T. Jeong, H.K. Park, K. Park, T.W. Na, E. Choi, The effect of Al to high-temperature deformation mechanisms and processing maps of Al0.5CoCrFeMnNi high entropy alloy, *J. Alloy. Compd.* 802 (2019) 152–165.
- [91] H.T. Jeong, H.K. Park, W.J. Kim, Hot deformation behavior and processing map of a Sn0.5CoCrFeMnNi high entropy alloy with dual phases, *Mater. Sci. Eng.: A* 801 (2021) 140394.
- [92] H.T. Jeong, W.J. Kim, Calculation and construction of deformation mechanism maps and processing maps for CoCrFeMnNi and Al0.5CoCrFeMnNi high-entropy alloys, *J. Alloy. Compd.* 869 (2021) 159256.
- [93] R. Fernández, G. González-Doncel, Threshold stress and load partitioning during creep of metal matrix composites, *Acta Mater.* 56 (11) (2008) 2549–2562.
- [94] R.A. Michi, J.P. Toinin, D.N. Seidman, D.C. Dunand, Ambient-and elevated-temperature strengthening by Al<sub>3</sub>Zr-Nanoprecipitates and Al<sub>3</sub>Ni-Microfibers in a cast Al-2.9Ni-0.11Zr-0.02Si-0.005Er (at%) alloy, *Mater. Sci. Eng. A* 759 (2019) 78–89.
- [95] H. Khodashenas, H. Mirzadeh, M. Malekan, M. Emamy, Constitutive modeling of flow stress during hot deformation of Sn-Al-Zn-Cu-Mg multi-principal-element alloy, *Vacuum* 170 (2019) 108970.
- [96] Y.C. Lin, X.M. Chen, A critical review of experimental results and constitutive descriptions for metals and alloys in hot working, *Mater. Des.* 32 (4) (2011) 1733–1759.
- [97] J. Zhang, C. Wu, Y. Peng, X. Xia, J. Li, J. Ding, C. Liu, X. Chen, J. Dong, Y. Liu, Hot compression deformation behavior and processing maps of ATI 718Plus superalloy, *J. Alloy. Compd.* 835 (2020) 155195.
- [98] Z. Gronostajski, The constitutive equations for FEM analysis, *J. Mater. Process. Technol.* 106 (1–3) (2000) 40–44.
- [99] D. Samantaray, S. Mandal, A.K. Bhaduri, P.V. Sivaprasad, An overview on constitutive modelling to predict elevated temperature flow behaviour of fast reactor structural materials, *Trans. Indian Inst. Met.* 63 (6) (2010) 823–831.
- [100] C. Brown, T. McCarthy, K. Chadha, S. Rodrigues, C. Aranas Jr., G.C. Saha, Constitutive modeling of the hot deformation behavior of CoCrFeMnNi high-entropy alloy, *Mater. Sci. Eng. A* 826 (2021) 141940.
- [101] T.W. Zhang, Z.M. Jiao, Z.H. Wang, J.W. Qiao, Dynamic deformation behaviors and constitutive relations of an AlCoCr1.5Fe1.5NiTi0.5 high-entropy alloy, *Scr. Mater.* 136 (2017) 15–19.

- [102] X. He, L. Liu, T. Zeng, Y. Yao, Micromechanical modeling of work hardening for coupling microstructure evolution, dynamic recovery and recrystallization: application to high entropy alloys, *Int. J. Mech. Sci.* 177 (2020) 105567.
- [103] H. Mirzadeh, A simplified approach for developing constitutive equations for modeling and prediction of hot deformation flow stress, *Metall. Mater. Trans. A* 46 (9) (2015) 4027–4037.
- [104] H. Rastegari, M. Rakhshkhorshid, M.C. Soman, D.A. Porter, Constitutive modeling of warm deformation flow curves of an eutectoid steel, *J. Mater. Eng. Perform.* 26 (5) (2017) 2170–2178.
- [105] M. Shalbafi, R. Roumina, R. Mahmudi, Hot deformation of the extruded Mg–10Li–1Zn alloy: constitutive analysis and processing maps, *J. Alloy. Compd.* 696 (2017) 1269–1277.
- [106] H.L. Wei, G.Q. Liu, M.H. Zhang, Physically based constitutive analysis to predict flow stress of medium carbon and vanadium microalloyed steels, *Mater. Sci. Eng. A* 602 (2014) 127–133.
- [107] H. Mirzadeh, Constitutive modeling and prediction of hot deformation flow stress under dynamic recrystallization conditions, *Mech. Mater.* 85 (2015) 66–79.
- [108] C. Lu, J. Shi, J. Wang, Physically based constitutive modeling for Ti17 alloy with original basketweave microstructure in  $\beta$  forging: a comparison of three approaches, *Mater. Charact.* 181 (2021) 111455.
- [109] P. Opela, I. Schindler, P. Kawulok, R. Kawulok, S. Ruzz, K. Rodak, Hot flow curve description of CuFe<sub>2</sub> alloy via different artificial neural network approaches, *J. Mater. Eng. Perform.* 28 (8) (2019) 4863–4870.
- [110] S.A. Sani, G.R. Ebrahimi, H. Vafaeenezhad, A.R. Kiani-Rashid, Modeling of hot deformation behavior and prediction of flow stress in a magnesium alloy using constitutive equation and artificial neural network (ANN) model, *J. Magnes. Alloy.* 6 (2) (2018) 134–144.
- [111] H. Ahmadi, H.R. Ashtiani, M. Heidari, A comparative study of phenomenological, physically-based and artificial neural network models to predict the hot flow behavior of API 5CT-L80 steel, *Mater. Today Commun.* 25 (2020) 101528.
- [112] S. Mandal, P.V. Sivaprasad, S. Venugopal, Capability of a feed-forward artificial neural network to predict the constitutive flow behavior of as cast 304 stainless steel under hot deformation, *J. Eng. Mater. Technol.* 129 (2007) 242–247.
- [113] Y.C. Lin, J. Zhang, J. Zhong, Application of neural networks to predict the elevated temperature flow behavior of a low alloy steel, *Comput. Mater. Sci.* 43 (4) (2008) 752–758.
- [114] H. Mirzadeh, J.M. Cabrera, A. Najafizadeh, Modeling and prediction of hot deformation flow curves, *Metall. Mater. Trans. A* 43 (1) (2012) 108–123.
- [115] F.J. Zerilli, R.W. Armstrong, Dislocation-mechanics-based constitutive relations for material dynamics calculations, *J. Appl. Phys.* 61 (5) (1987) 1816–1825.
- [116] T. Mirzaie, H. Mirzadeh, J.M. Cabrera, A simple Zerilli–Armstrong constitutive equation for modeling and prediction of hot deformation flow stress of steels, *Mech. Mater.* 94 (2016) 38–45.
- [117] D. Samantaray, S. Mandal, U. Borah, A.K. Bhaduri, P.V. Sivaprasad, A thermoviscoplastic constitutive model to predict elevated-temperature flow behaviour in a titanium-modified austenitic stainless steel, *Mater. Sci. Eng. A* 526 (1–2) (2009) 1–6.
- [118] Y.C. Lin, X.M. Chen, A combined Johnson–Cook and Zerilli–Armstrong model for hot compressed typical high-strength alloy steel, *Comput. Mater. Sci.* 49 (3) (2010) 628–633.
- [119] R. Bobbili, V. Madhu, Physically-based constitutive model for flow behavior of a Ti–22Al–25Nb alloy at high strain rates, *J. Alloy. Compd.* 762 (2018) 842–848.
- [120] C. Brown, T. McCarthy, K. Chadha, S. Rodrigues, C. Aranas Jr., G.C. Saha, Constitutive modeling of the hot deformation behavior of CoCrFeMnNi high-entropy alloy, *Mater. Sci. Eng. A* 826 (2021) 141940.
- [121] A.P.D.B. Guerra, A.M. Jorge, V. Roche, C. Bolfarini, Hot deformation behavior of a beta metastable TMZF alloy: microstructural and constitutive phenomenological analysis, *Metals* 11 (11) (2021) 1769.
- [122] G.R. Johnson, W.H. Cook, 1983. A constitutive model and data for metals subjected to large strains, high strain rates and high temperatures. Proceedings of the Seventh International Symposium on Ballistic, The Hague, The Netherlands, 541–547.
- [123] Z. Akbari, H. Mirzadeh, J.M. Cabrera, A simple constitutive model for predicting flow stress of medium carbon microalloyed steel during hot deformation, *Mater. Des.* 77 (2015) 126–131.
- [124] Y. Wang, X. Zeng, H. Chen, X. Yang, F. Wang, L. Zeng, Modified Johnson–Cook constitutive model of metallic materials under a wide range of temperatures and strain rates, *Results Phys.* 27 (2021) 104498.
- [125] Y.C. Lin, X.M. Chen, G. Liu, A modified Johnson–Cook model for tensile behaviors of typical high-strength alloy steel, *Mater. Sci. Eng.: A* 527 (26) (2010) 6980–6986.
- [126] R. Bobbili, V. Madhu, A modified Johnson–Cook model for FeCoNiCr high-entropy alloy over a wide range of strain rates, *Mater. Lett.* 218 (2018) 103–105.
- [127] X.M. Chen, Y.C. Lin, H.W. Hu, S.C. Luo, X.J. Zhou, Y. Huang, An enhanced Johnson–Cook model for hot compressed A356 aluminum alloy, *Adv. Eng. Mater.* 23 (1) (2021) 2000704.
- [128] A. Hensel, T. Spittel, 1978. *Kraft- und Arbeitsbedarf bildsamer Formgebungsverfahren*. VEB Deutscher Verlag für Grundstoffindustrie, Leipzig.
- [129] J.D. Yoo, M.C. Kim, E.J. Kim, M.K. Razali, M.S. Joun, Flow stress characterization of magnesium alloys at elevated temperatures: A review, *J. Phys. Conf. Ser.* 2047 (1) (2021) 012002.
- [130] S. Spigarelli, M. El Mehmedi, A new constitutive model for the plastic flow of metals at elevated temperatures, *J. Mater. Eng. Perform.* 23 (2) (2014) 658–665.
- [131] Z.J. Chen, Y.C. Lin, D.G. He, Y.M. Lou, M.S. Chen, A unified dislocation density-based model for an aged polycrystalline Ni-based superalloy considering the coupled effects of complicate deformation mechanisms and initial  $\delta$  phase, *Mater. Sci. Eng. A* 827 (2021) 142062.
- [132] Y.W. Xiao, Y.C. Lin, Y.Q. Jiang, X.Y. Zhang, G.D. Pang, D. Wang, K.C. Zhou, A dislocation density-based model and processing maps of Ti-55511 alloy with bimodal microstructures during hot compression in  $\alpha+\beta$  region, *Mater. Sci. Eng. A* 790 (2020) 139692.
- [133] U.F. Kocks, H. Mecking, Physics and phenomenology of strain hardening: the FCC case, *Prog. Mater. Sci.* 48 (3) (2003) 171–273.
- [134] Z. Nasiri, S. Ghaemifar, M. Naghizadeh, H. Mirzadeh, Thermal mechanisms of grain refinement in steels: a review, *Met. Mater. Int.* 27 (7) (2021) 2078–2094.
- [135] M.J. Sohrabi, M. Naghizadeh, H. Mirzadeh, Deformation-induced martensite in austenitic stainless steels: a review, *Arch. Civ. Mech. Eng.* 20 (4) (2020) 124.
- [136] M.S. Mehranpour, H. Shahmir, M. Nili-ahmadabadi, CoCrFeNiMn high entropy alloy microstructure and mechanical properties after severe cold shape rolling and annealing, *Mater. Sci. Eng.: A* 793 (2020) 139884.
- [137] R. Zamani, H. Mirzadeh, M. Emamy, Mechanical properties of a hot deformed Al-Mg2Si in-situ composite, *Mater. Sci. Eng. A* 726 (2018) 10–17.
- [138] B. Pourbahrari, H. Mirzadeh, M. Emamy, Elucidating the effect of intermetallic compounds on the behavior of Mg–Gd–Al–Zn magnesium alloys at elevated temperatures, *J. Mater. Res.* 32 (22) (2017) 4186–4195.
- [139] H. Mirzadeh, High strain rate superplasticity via friction stir processing (FSP): a review, *Mater. Sci. Eng. A* 819 (2021) 141499.
- [140] Z. Nasiri, M.S. Khorrami, H. Mirzadeh, M. Emamy, Enhanced mechanical properties of as-cast Mg-Al-Ca magnesium alloys by friction stir processing, *Mater. Lett.* 296 (2021) 129880.
- [141] A. Heidarzadeh, S. Mironov, R. Kaibyshev, G. Çam, A. Simar, A. Gerlich, F. Khodabakhshi, A. Mostafaee, D.P. Field, J.D. Robson, A. Deschamps, P.J. Withers, Friction stir welding/processing of metals and alloys: a comprehensive review on microstructural evolution, *Prog. Mater. Sci.* 117 (2021) 100752.
- [142] T. Wang, S. Shukla, M. Komarasamy, K. Liu, R.S. Mishra, Towards heterogeneous AlxCrFeNi high entropy alloy via friction stir processing, *Mater. Lett.* 236 (2019) 472–475.
- [143] S.S. Nene, K. Liu, M. Frank, R.S. Mishra, R.E. Brennan, K.C. Cho, Z. Li, D. Raabe, Enhanced strength and ductility in a friction stir processing engineered dual phase high entropy alloy, *Sci. Rep.* 7 (1) (2017) 16167.
- [144] N.T.C. Nguyen, P. Asghari-Rad, P. Sathiyamoorthi, A. Zargaran, C.S. Lee, H.S. Kim, Ultrahigh high-strain-rate superplasticity in a nanostructured high-entropy alloy, *Nat. Commun.* 11 (1) (2020) 2736.
- [145] S.R. Reddy, S. Bapari, P.P. Bhattacharjee, A.H. Chokshi, Superplastic-like flow in a fine-grained equiatomic CoCrFeMnNi high-entropy alloy, *Mater. Res. Lett.* 5 (6) (2017) 408–414.
- [146] H.T. Jeong, W.J. Kim, Calculation and construction of deformation mechanism maps and processing maps for CoCrFeMnNi and Al<sub>0.5</sub>CoCrFeMnNi high-entropy alloys, *J. Alloy. Compd.* 869 (2021) 159256.
- [147] H. Shahmir, M. Nili-Ahmabadabi, A. Shafee, T.G. Langdon, Effect of a minor titanium addition on the superplastic properties of a CoCrFeNiMn high-entropy alloy processed by high-pressure torsion, *Mater. Sci. Eng. A* 718 (2018) 468–476.
- [148] S.S. Nene, K. Liu, S. Sinha, M. Frank, S. Williams, R.S. Mishra, Superplasticity in fine grained dual phase high entropy alloy, *Materialia* 9 (2020) 100521.
- [149] S.S. Sohn, D.G. Kim, Y.H. Jo, A.K. da Silva, W. Lu, A.J. Breen, B. Gault, D. Ponge, High-rate superplasticity in an equiatomic medium-entropy VCoNi alloy enabled through dynamic recrystallization of a duplex microstructure of ordered phases, *Acta Mater.* 194 (2020) 106–117.
- [150] T. Cao, W. Guo, W. Lu, Y. Xue, W. Lu, J. Su, C.H. Liebscher, C. Li, G. Dehm, Strain rate dependent deformation behavior of BCC-structured Ti<sub>29</sub>Zr<sub>24</sub>Nb<sub>23</sub>Hf<sub>24</sub> high entropy alloy at elevated temperatures, *J. Alloy. Compd.* 891 (2022) 161859.
- [151] H. Mirzadeh, Quantification of the strengthening effect of rare earth elements during hot deformation of Mg–Gd–Y–Zr magnesium alloy, *J. Mater. Res. Technol.* 5 (1) (2016) 1–4.
- [152] H. Mirzadeh, Constitutive behaviors of magnesium and Mg–Zn–Zr alloy during hot deformation, *Mater. Chem. Phys.* 152 (2015) 123–126.
- [153] H. Mirzadeh, Quantification of the strengthening effect of reinforcements during hot deformation of aluminum-based composites, *Mater. Des.* 65 (2015) 80–82.
- [154] J. Li, B. Gao, S. Tang, B. Liu, Y. Liu, Y. Wang, J. Wang, High temperature deformation behavior of carbon-containing FeCoCrNiMn high entropy alloy, *J. Alloy. Compd.* 747 (2018) 571–579.
- [155] J.P. Sah, G.J. Richardson, C.M. Sellars, Grain-size effects during dynamic recrystallization of nickel, *Met. Sci.* 8 (1) (1974) 325–331.
- [156] S.M. Fatemi-Varzaneh, A. Zarei-Hanzaki, H. Beladi, Dynamic recrystallization in AZ31 magnesium alloy, *Mater. Sci. Eng.: A* 456 (1–2) (2007) 52–57.
- [157] F.J. Humphreys, G.S. Rohrer, A.D. Rollett, *Recrystallization and Related Annealing Phenomena*, third ed., Elsevier, Oxford, 2017.
- [158] S. Saadatkar, H. Mirzadeh, J.M. Cabrera, Hot deformation behavior, dynamic recrystallization, and physically-based constitutive modeling of plain carbon steels, *Mater. Sci. Eng.: A* 636 (2015) 196–202.
- [159] T. Sakai, A. Belyakov, R. Kaibyshev, H. Miura, J.J. Jonas, Dynamic and post-dynamic recrystallization under hot, cold and severe plastic deformation conditions, *Prog. Mater. Sci.* 60 (2014) 130–207.
- [160] Z.X. Zhang, S.Q. Qu, A.H. Feng, J. Shen, D.L. Chen, Hot deformation behavior of Ti-6Al-4V alloy: Effect of initial microstructure, *J. Alloy. Compd.* 718 (2017) 170–181.
- [161] A. Dehghan-Manshadi, P.D. Hodgson, Dependency of recrystallization mechanism to the initial grain size, *Metall. Mater. Trans. A* 39 (12) (2008) 2830–2840.

- [162] M. El Wahabi, L. Gavard, F. Montheillet, J.M. Cabrera, J.M. Prado, Effect of initial grain size on dynamic recrystallization in high purity austenitic stainless steels, *Acta Mater.* 53 (17) (2005) 4605–4612.
- [163] H. Zhang, Y. Zhang, H. Liang, L. Yu, Y. Liu, Effect of the primary O phase on thermal deformation behavior of a Ti<sub>2</sub>AlNb-based alloy, *J. Alloy. Compd.* 846 (2020) 156458.
- [164] R. Ebrahimi, S. Solhjoo, Characteristic points of stress-strain curve at high temperature, *Int. J. Iron Steel Soc. Iran.* 4 (1) (2007) 24–27.
- [165] A. Momeni, K. Dehghani, G.R. Ebrahimi, Modeling the initiation of dynamic recrystallization using a dynamic recovery model, *J. Alloy. Compd.* 509 (39) (2011) 9387–9393.
- [166] H. Mirzadeh, J.M. Cabrera, A. Najafizadeh, P.R. Calvillo, EBSD study of a hot deformed austenitic stainless steel, *Mater. Sci. Eng.: A* 538 (2012) 236–245.
- [167] A. Hadadzadeh, F. Mokdad, M.A. Wells, D.L. Chen, A new grain orientation spread approach to analyze the dynamic recrystallization behavior of a cast-homogenized Mg-Zn-Zr alloy using electron backscattered diffraction, *Mater. Sci. Eng. A* 709 (2018) 285–289.
- [168] S. Venugopal, S.L. Mannan, Y.V.R.K. Prasad, Influence of state of stress on the processing map for hot working of stainless steel type AISI 304L: compression vs. torsion, *Mater. Sci. Eng. A* 160 (1) (1993) 63–69.
- [169] Y.V.R.K. Prasad, K.P. Rao, S. Sasidhar, Hot Working Guide: A Compendium of Processing MMaps, ASM international, 2015.
- [170] S.V.S. Narayana Murty, B. Nageswara Rao, B.P. Kashyap, Instability criteria for hot deformation of materials, *Int. Mater. Rev.* 45 (1) (2000) 15–26.
- [171] I. Rieiro, M. Carsí, O.A. Ruano, A new stability criterion for the hot deformation behavior of materials: application to the AZ31 magnesium alloy, *Metall. Mater. Trans. A* 48 (7) (2017) 3445–3460.
- [172] H. Mirzadeh, Simple physically-based constitutive equations for hot deformation of 2024 and 7075 aluminum alloys, *Trans. Nonferrous Met. Soc. China* 25 (5) (2015) 1614–1618.
- [173] H. Mirzadeh, Constitutive modeling of commercial pure titanium during hot deformation in alpha and beta phase fields, *Indian J. Eng. Mater. Sci.* 23 (2016) 60–64.
- [174] X. Quellenec, N. Bozzolo, J.J. Jonas, R. Loge, A new approach to modeling the flow curve of hot deformed austenite, *ISIJ Int.* 51 (6) (2011) 945–950.
- [175] Y.C. Lin, X.M. Chen, D.X. Wen, M.S. Chen, A physically-based constitutive model for a typical nickel-based superalloy, *Comput. Mater. Sci.* 83 (2014) 282–289.
- [176] O. Jorge Junior, A. M., & Balancin, Prediction of steel flow stresses under hot working conditions, *Mater. Res.* 8 (2005) 309–315.
- [177] H. Mirzadeh, A. Najafizadeh, The rate of dynamic recrystallization in 17-4 PH stainless steel, *Mater. Des.* 31 (10) (2010) 4577–4583.
- [178] R. Bobbili, B.V. Ramudu, V. Madhu, A physically-based constitutive model for hot deformation of Ti-10-2-3 alloy, *J. Alloy. Compd.* 696 (2017) 295–303.
- [179] H. Mirzadeh, A. Najafizadeh, Extrapolation of flow curves at hot working conditions, *Mater. Sci. Eng. A* 527 (7–8) (2010) 1856–1860.
- [180] E.S. Puchi-Cabrera, J.D. Guérin, J.G. La Barbera-Sosa, M. Dubar, L. Dubar, Plausible extension of Anand's model to metals exhibiting dynamic recrystallization and its experimental validation, *Int. J. Plast.* 108 (2018) 70–87.
- [181] Y.Q. Jiang, Y.C. Lin, G.Q. Wang, G.D. Pang, M.S. Chen, Z.C. Huang, Microstructure evolution and a unified constitutive model for a Ti-55511 alloy deformed in  $\beta$  region, *J. Alloy. Compd.* 870 (2021) 159534.
- [182] E. Shafei, N. Goodarzi, K. Dehghani, A. Soltani Tehrani, A new constitutive equation to predict single peak flow stress curves at high temperatures: a comprehensive study on different steels, *Can. Metall. Q.* 56 (1) (2017) 104–112.
- [183] K.A. Babu, S. Mandal, Regression based novel constitutive analyses to predict high temperature flow behavior in super austenitic stainless steel, *Mater. Sci. Eng. A* 703 (2017) 187–195.
- [184] H. Mirzadeh, Developing constitutive equations of flow stress for hot deformation of AZ31 magnesium alloy under compression, torsion, and tension, *Int. J. Mater. Form.* 12 (4) (2019) 643–648.
- [185] A.B. Cota, R. Barbosa, D.B. Santos, Simulation of the controlled rolling and accelerated cooling of a bainitic steel using torsion testing, *J. Mater. Process. Technol.* 100 (1–3) (2000) 156–162.
- [186] A. Saboori, A. Abdi, S.A. Fatemi, G. Marchese, S. Biamino, H. Mirzadeh, Hot deformation behavior and flow stress modeling of Ti-6Al-4V alloy produced via electron beam melting additive manufacturing technology in single  $\beta$ -phase field, *Mater. Sci. Eng. A* 792 (2020) 139822.
- [187] S.I. Shakil, N.R. Smith, S.P. Yoder, B.E. Ross, D.J. Alvarado, A. Hadadzadeh, M. Haghshenas, Post fabrication thermomechanical processing of additive manufactured metals: a review, *J. Manuf. Process.* 73 (2022) 757–790.
- [188] K. Moeinfar, F. Khodabakhshi, S.F. Kashani-bozorg, M. Mohammadi, A.P. Gerlich, A review on metallurgical aspects of laser additive manufacturing (LAM): stainless steels, nickel superalloys, and titanium alloys, *J. Mater. Res. Technol.* 16 (2022) 1029–1068.
- [189] Y.K. Kim, S. Yang, K.A. Lee, Superior temperature-dependent mechanical properties and deformation behavior of equiatomic CoCrFeMnNi high-entropy alloy additively manufactured by selective laser melting, *Sci. Rep.* 10 (1) (2020) 1–13.
- [190] D. Lin, X. Xi, X. Li, J. Hu, L. Xu, Y. Han, Y. Zhang, L. Zhao, High-temperature mechanical properties of FeCoCrNi high-entropy alloys fabricated via selective laser melting, *Mater. Sci. Eng. A* (2021) 142354.